

## INFORMATION TO USERS

The most advanced technology has been used to photograph and reproduce this manuscript from the microfilm master. UMI films the text directly from the original or copy submitted. Thus, some thesis and dissertation copies are in typewriter face, while others may be from any type of computer printer.

**The quality of this reproduction is dependent upon the quality of the copy submitted.** Broken or indistinct print, colored or poor quality illustrations and photographs, print bleedthrough, substandard margins, and improper alignment can adversely affect reproduction.

In the unlikely event that the author did not send UMI a complete manuscript and there are missing pages, these will be noted. Also, if unauthorized copyright material had to be removed, a note will indicate the deletion.

Oversize materials (e.g., maps, drawings, charts) are reproduced by sectioning the original, beginning at the upper left-hand corner and continuing from left to right in equal sections with small overlaps. Each original is also photographed in one exposure and is included in reduced form at the back of the book.

Photographs included in the original manuscript have been reproduced xerographically in this copy. Higher quality 6 x 9" black and white photographic prints are available for any photographs or illustrations appearing in this copy for an additional charge. Contact UMI directly to order.

# UMI

University Microfilms International  
300 North Zeeb Road  
Ann Arbor, MI 48106-1500  
Tel: 734/769-0900

Order Number 1341913

**Mechanisms of chemical suppression of rocket exhaust  
afterburning**

McMillon, Leshe Glen, Jr., M.S.

University of Nevada, Reno, 1990

**U·M·I**

300 N Zeeb Rd  
Ann Arbor, MI 48106

University of Nevada

Reno

Mechanisms of Chemical Suppression  
of Rocket Exhaust Afterburning

A thesis submitted in partial fulfillment of the  
requirements for the degree of  
Master of Science in Metallurgical Engineering

by

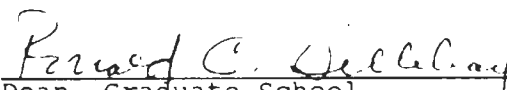
Leslie Glen McMillion, Jr.

July 1990

The thesis of Leslie Glen McMillion, Jr. is approved:

  
\_\_\_\_\_  
Thesis Advisor

  
\_\_\_\_\_  
Department Chair

  
\_\_\_\_\_  
Dean, Graduate School

University of Nevada

Reno

July 1990

## ACKNOWLEDGEMENTS

The author gratefully acknowledges the financial and professional support of the Thiokol Corporation (formerly Morton Thiokol, Inc., Aerospace Group) and particularly the involvement of Mr. Tom Davidson and Dr. Dave Flanigan, both of whom were tremendously helpful. Also, the encouragement of Professor Eugene Miller must be acknowledged; his contributions went far beyond "just doing his job."

## ABSTRACT

Mechanisms of Chemical Suppression  
of Rocket Exhaust Afterburning

by

Leslie Glen McMillion, Jr.

Methyl bromide, anhydrous ammonia, and phosphorus pentoxide were added to flat, laminar, opposed-jet diffusion flames of  $\text{CH}_4\text{-O}_2\text{-N}_2$  and  $\text{H}_2\text{-CO-O}_2\text{-N}_2$ . The  $4000\text{ cm}^{-1}$  to  $2000\text{ cm}^{-1}$  infrared flame emission spectra were scanned in non-overlapping increments of 0.33 mm width using a modified infrared absorption spectrometer with an external optical scanning system. Methyl bromide results show narrowing of the flame zone and an increase in maximum emission intensity. This is consistent with studies in the literature and validates the use of opposed-jet flames for evaluating additive effects. Ammonia results show inhibition occurring on the fuel side of the flames and acceleration occurring on the oxygen side. Phosphorus pentoxide results show behavior that is interpreted as resulting from non-equilibrium processes in the flames, which prevents drawing conclusions about phosphorus pentoxide effects on afterburning. The practicality of using these additives in solid propulsion systems is discussed.

TABLE OF CONTENTS

ACKNOWLEDGEMENTS . . . . . iii

ABSTRACT . . . . . iv

INTRODUCTION . . . . . 1

THEORY AND LITERATURE REVIEW . . . . . 5

    Chemical Kinetics . . . . . 5

    Equilibria, Radiation and Collision Processes . . . . . 8

    Flame Temperature . . . . . 10

    Oxidation Mechanism of Hydrogen/Carbon Monoxide . . . . . 13

    Oxidation Mechanism of Methane . . . . . 15

    Oxidation Mechanism of Ammonia . . . . . 16

    Inhibition Mechanisms of Specific Compounds . . . . . 18

        Bromides . . . . . 18

        Ammonia . . . . . 22

        Phosphorus Pentoxide . . . . . 25

EXPERIMENTAL APPARATUS AND METHOD . . . . . 28

EXPERIMENTAL RESULTS . . . . . 33

    Methyl Bromide . . . . . 35

    Ammonia . . . . . 40

    Phosphorus Pentoxide . . . . . 42

DISCUSSION . . . . . 44

    Methyl Bromide . . . . . 44

    Ammonia . . . . . 47

    Phosphorus Pentoxide . . . . . 50

    Applications to Solid Propulsion . . . . . 53

CONCLUSIONS . . . . . 55

    Methyl Bromide . . . . . 55

    Ammonia . . . . . 56

    Phosphorus Pentoxide . . . . . 56

    Applications to Solid Propulsion . . . . . 57

REFERENCES . . . . . 58

TABLES OF OXIDATION MECHANISMS . . . . . 63

TABLES OF EXPERIMENTAL RESULTS . . . . . 67

FIGURES . . . . . 86

## INTRODUCTION

In recent years the armed services have increasingly emphasized the development and use of low signature tactical solid rocket motors. Visible primary and secondary smoke have been virtually eliminated by the removal of metal powder additives, ammonium perchlorate, and most of the ballistic modifiers from the propellant formulations resulting in "minimum smoke" propellants.<sup>1</sup> However, the exhaust gases from minimum smoke propellants contain large concentrations of hydrogen and carbon monoxide. When mixed with ambient air in the plume, the hydrogen and carbon monoxide burn to form water and carbon dioxide. The results are visible flash, increased ultraviolet radiation, and increased infrared radiation.<sup>2</sup> This so-called "afterburning" can temporarily blind the gunner, interferes with optical guidance systems, and increases observability, thus decreasing the survivability of the launch platform. Afterburning also increases the propensity for contrail (secondary smoke) formation; some of the secondary smoke advantage of minimum-smoke propellants over "reduced-smoke" propellants is lost because the hydrogen in the plume reacts to form additional water which is available for potential condensation to smoke.<sup>3</sup> Reduced smoke propellants use ammonium perchlorate oxidizer with low solids content, and more easily form contrails because HCl in the exhaust lowers the equilibrium vapor pressure of water in the plume.

There are several methods by which afterburning can be suppressed. These include the use of chemical additives, reduction of rocket exhaust gas temperature, reduction of the  $H_2/CO$  concentrations in the plume, or combinations of the above.

Many chemicals inhibit the combustion of hydrogen and carbon monoxide. The mechanism is generally agreed to involve removal of active species, such as H atoms, OH radicals, and O atoms. Many chemicals, mostly inorganic salts, have been evaluated as potential afterburning suppressants.<sup>4</sup> Potassium salts such as  $K_2SO_4$  and  $KNO_3$ , which have been found to be most effective, have been added to propellant charges to suppress gun muzzle flash and rocket plume infrared signature.<sup>5,6</sup> Even though potassium salts suppress afterburning, they are not ideal propellant additives because they produce primary smoke, increase the formation of secondary smoke, and they can increase the concentration of electrons and detectable ionized species in the plume.

This work is directed at understanding the mechanisms of chemical suppression of rocket exhaust afterburning through evaluation of different additives which are known to influence the reaction rate of combustion systems. Identification of practical additives for propulsion systems was not a primary goal of this study, but rather the elucidation of the mechanisms of afterburning inhibition.

Three additives were chosen for evaluation. They were methyl bromide, phosphorus pentoxide, and anhydrous ammonia.

Methyl bromide was chosen because it is a known inhibitor and many studies on its effects appear in the open literature. Phosphorus was evaluated because organo-phosphorus compounds have been used as flame retardants in textiles and plastics, and as anti-knock additives in gasoline; phosphorus pentoxide (written as  $P_2O_5$  or  $P_4O_{10}$ ) was chosen because it sublimates with a relatively high vapor pressure at easily attained temperatures. There is evidence of suppression of afterburning by ammonium salts and amines. Also, the interest in environmental  $NO_x$  chemistry made ammonia a good choice because many studies on ammonia chemistry in combustion have been published.

Methyl bromide, phosphorus pentoxide, and anhydrous ammonia were introduced into atmospheric pressure, flat, laminar, opposed-jet diffusion flames of hydrogen/carbon monoxide with oxygen, and methane with oxygen. Nitrogen was used as a diluent. The flame emission zones were scanned incrementally to examine the infrared spectral emissions. An infrared spectrometer with an external optical system permitted examination of the spectra from narrow segments of the flames. An opposed-jet diffusion burner adapted from one described by Hahn, Wendt, and Tyson<sup>7</sup> was used. The opposed-jet diffusion flame exhibits a broad reaction zone which enhanced the ability to study the effects of additives.

The data collected by examining the spectral and spatial infrared emissions from opposed-jet diffusion flames were not directed toward the measurement of kinetic rates. To provide

a basis for a definitive evaluation of kinetic rates, species concentrations and temperatures would have to be measured. Since this work did not measure flame temperature nor concentration profiles that can be correlated with the measured infrared spectra, there is no way to separate their effects on the radiative intensity. A change in radiative intensity, which is taken to be directly proportional to spectral area, can result from a change in temperature at constant emitter concentration, a change in concentration at constant temperature, or both. Because of this inability to determine values needed for kinetics studies, the use of kinetics in the following explanations of the effects of additives on spectral and spatial infrared flame emissions are based on interpretation of the literature summarized below.

The spectral data are of value for identifying emitters. The strongest infrared emissions are due to  $H_2O$  and  $CO_2$ . The intermediate species  $OH$ ,  $CO$ ,  $CH_3$ , and  $HCHO$  are infrared active, but their emissions cannot be isolated from the recorded spectra due to band overlap with  $H_2O$  and  $CO_2$ .

## THEORY AND LITERATURE REVIEW

### Chemical Kinetics

Combustion reactions fall into several categories: auto-oxidations, pure decomposition reactions, and fuel-oxidant reactions.<sup>8</sup> Combustion processes are the result of simultaneous, interdependent reactions termed chain reactions. Except at very high temperatures, the main chain carriers are uncharged free atoms or radicals.<sup>8</sup> The work presented here deals with fuel-oxidant reactions and considers uncharged species only.

Chain reactions have several steps: initiating, propagating, branching, and termination. Each step consists of one or more reactions. The chain initiating step generates chain carriers, usually through thermal two-body collisions or photochemical decomposition. The chain propagating steps generate products with no net change in the number of chain carriers. The chain branching step allows a system to achieve a nonthermal explosion by creating more chain carriers than are consumed. The chain termination step results in a net loss of chain carriers. In enclosed systems at low pressures, radicals are destroyed at the walls. However, in a system such as the opposed-jet diffusion burner or a rocket exhaust, surface destruction of free radicals is unimportant, and the main route for chain termination is through recombination of radicals in the gas phase by three-body collisions, which

consume two chain carriers and form either product or reactant species.<sup>9</sup>

Factors which determine the rate at which a chemical reaction proceeds include the concentration of reactants, the temperature, the presence of energy absorbing or providing species, and the presence of a catalyst or inhibitor. The rate of reaction is usually expressed in terms of the concentration of reactants and a reaction rate coefficient. The Arrhenius form of the rate coefficient is written as

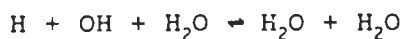
$$k = A T^a \exp(-E_a/RT)$$

where A is a constant that takes into account the collision diameter and reduced mass for the reacting species, and the steric factor. The term  $\exp(-E_a/RT)$  is the Boltzmann factor, which specifies the fraction of all collisions that have energy greater than the activation energy,  $E_a$ , required for the reaction to proceed.

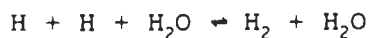
For free radical reactions, the activation energy is very small, 0 to 5 kcal/mole. Thus the exponential term approaches unity and the temperature dependence of the preexponential term becomes more important.<sup>10</sup>

A great deal of energy is liberated through radical recombination. This energy is often sufficient to cause the product to decompose into the original radicals. Thus collision with a third body is required to remove enough energy to stabilize the product.<sup>11</sup> For example, in hydrogen

flames the most important processes for radical recombination are considered to be <sup>12</sup>



and



where  $\text{H}_2\text{O}$  is a very efficient energy absorber.

For termolecular reactions at higher temperatures, the rate coefficient can usually be expressed as <sup>13</sup>

$$k = A (1/T)$$

where  $A$  is a constant. This expression is the Arrhenius equation with  $a = -1$  and  $E_A$  near zero. The simple inverse temperature dependence shows that the rate of termolecular reactions decreases with increasing temperature. <sup>12</sup>

At temperatures below 750K-1000K there is a region of slow reaction where the presence of inhibitors can have effects on the rate and relative proportions of intermediate species and products. <sup>8</sup> The inhibition of combustion is due to competitive reaction kinetics among the reactions that generate free radicals and the inhibition reactions that consume them. The effects of inhibition are most significant at the relatively low preflame temperatures for the methane and hydrogen/carbon monoxide systems. For this reason charged species, which occur in significant quantities only at higher

temperatures, <sup>14</sup> are not considered in the following discussions of combustion mechanisms.

### Equilibria, Radiation and Collision Processes

The theory of equilibria and radiation is discussed in detail by Gaydon. <sup>15</sup> The strength of emission of a spectrum band depends on the concentration of emitters in the appropriate excited state, the rate at which radiation occurs from that state, and the degree of self-absorption occurring in the system. If the gases are in thermodynamic equilibrium, the number of molecules in an excited state can be related to the number in the ground state for a specified temperature by the Maxwell-Boltzmann distribution law. Higher temperatures result in larger ratio of excited species to ground state species.

The infrared radiation from steady flames that do not form soot appears to be mainly thermal from infrared active vibrational and rotational modes of flame gases. Generally, the long radiative lifetime for transitions in the infrared allow time for collisions to establish thermal and chemical equilibria before the molecule radiates. However, there is evidence that non-equilibrium effects can occur. Molecules can be formed in an excited thermal state by chemical processes, or be excited above equilibrium levels by collision with a chemically-formed excited molecule. Deviations from chemical equilibrium can also occur.

The emission from any material cannot exceed that from a blackbody at the same temperature. The sensitivity of individual band emission intensity to changes in temperature is affected, however, by the emissivity of the gas and the optical thickness of the flame. For the emission band in the region 2450-2000  $\text{cm}^{-1}$ ,  $\text{CO}_2$  emissivity is about 0.8 at 2220K and for an optical depth of 0.7  $\text{cm-atm}$ .<sup>16</sup> For an optical depth of 0.3  $\text{cm-atm}$  at 2200K, the emissivity of water in the spectral region examined in the present work is about 0.1.<sup>17</sup> The greater emissivity of  $\text{CO}_2$  in the region studied makes the optical depth of  $\text{CO}_2$  greater than for  $\text{H}_2\text{O}$ .  $\text{CO}_2$  emission intensity is thus less sensitive than  $\text{H}_2\text{O}$  emission to changes in temperature and concentration because  $\text{CO}_2$  is behaving more like a black body. This behavior is seen in the experimental results presented below.

The appearance and structure of flame infrared emission bands are greatly modified by self-absorption. At higher temperatures, the large population of upper vibrational and rotational transitions broaden the emission bands and smear out the fine structure resulting in a virtually continuous band. Absorption by  $\text{H}_2\text{O}$  and  $\text{CO}_2$  in the cooler outer layers of the flame and in the atmosphere weakens the centers of the bands and the maximum intensity is displaced to longer wavelengths. The extent of absorption depends on the flame shape and size, and the path length through the atmosphere.

Thermal equilibrium, chemical equilibrium, and a constant degree of self-absorption are assumed in the following

discussions of experimental results. These assumptions are the basis for the interpretation of changes in species spectral radiation area as indicating changes in temperature and/or concentrations resulting from alterations in the relative reaction rates. As will be seen, these assumptions may not hold in the case of phosphorus pentoxide. The  $P_4O_{10}$  results show unusual characteristics which may be due to non-equilibrium effects.

### Flame Temperature

Chemical and thermal equilibrium are normally assumed in the evaluation of combustion systems. A detailed review of chemical thermodynamics as applied to combustion systems is presented in reference 18.

When the energy evolved by combustion reactions is used solely to raise the product temperature, this temperature is called the adiabatic flame temperature; under no circumstances can the temperature of the flame exceed the adiabatic flame temperature. In practice, the adiabatic flame temperature is not reached for laboratory flames whose temperature exceeds about 1250K. At high temperatures, energy is absorbed by dissociation and ionization reactions. Dissociation and ionization reactions are highly endothermic and a few percent dissociation or ionization can lower the flame temperature substantially. Also, energy is lost to the surroundings by radiation, convection, and conduction; the amount of energy

lost depends on the configuration of the flame. The maximum temperature of practical flames depends on many variables and may cover a range of values, but it cannot exceed the adiabatic flame temperature.

A useful parameter for describing combustion systems is the equivalence ratio,  $\phi$ . It is defined as the ratio of fuel-to-oxidizer of the system being studied divided by the stoichiometric fuel-to-oxidizer ratio for the same fuel and oxidizer:

$$\phi = (F/O)/(F/O)_{\text{stoich}}$$

The main reaction zone in a diffusion flame forms where the fuel and oxidizer are present in approximately stoichiometric proportions. The overall equivalence ratio affects concentration profiles, diffusion rates, and consequently, flame width and temperature profiles.

The temperature profile in a flat, laminar, opposed-jet diffusion flame is affected by aerodynamics, the heats of formation of fuel and oxidizer, the flow rates of fuel and oxidizer, the equivalence ratio, the amount of diluent, and the efficiency of heat transfer by radiation and conduction. The amount of energy available for heating the flame gases is fixed by the heats of formation and amounts of fuel and oxidizer. The temperature reached by the system is determined by how this fixed amount of energy is distributed.

For a specified flow rate of fuel and oxidizer, the energy released in the flame is fixed, assuming chemical equilibrium is achieved. The flame width and maximum temperature are affected by the amount of diluent, the velocity of the gas streams, and the heat losses to the surroundings. An undiluted system will reach higher temperatures than a dilute system because of the heat capacity of the diluent. A dilute flame will be broader than a flame with less diluent because the diluent slows the reaction rate by reducing the collision probability between reactive species.

The width of the flame zone is strongly affected by the linear velocity of the gas streams for the opposed-jet burner. If the flow rates are low, a broad flame zone forms. Higher flow rates compress the volume into which the heat of combustion is released. A broad flame will be cooler than a narrow flame because the narrow flame has the same amount of energy heating a smaller volume of gas.

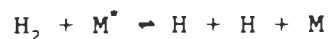
The results presented here show an increase in infrared spectral radiation upon addition of methyl bromide and ammonia at constant linear velocity of the gas streams. This is reasonable because of an increase in average temperature resulting from an observed decrease in flame width. The  $P_4O_{10}$  results, however, show an increase in both flame width and infrared spectral radiation. This is contradictory to the principles outlined above, but it is possibly due to non-

equilibrium effects. Explanations for these behaviors are presented below.

#### Oxidation Mechanism of Hydrogen/Carbon Monoxide

The predominant steps in oxidation of hydrogen and carbon monoxide are shown in Table I along with forward and reverse rate coefficients,  $k$ , at 700K and 1750K. The rate coefficients at 700K apply to the low temperature region at the edges of the flames, and the coefficients at 1750K to the higher temperature main reaction zone. The rate coefficients were calculated from data presented by Hahn and Wendt<sup>19</sup> after Levy, Longwell, Sarofim, Corley, Heap, and Tyson.<sup>20</sup> The specie designated "M" is an energy-removing collision partner such as CO<sub>2</sub>, H<sub>2</sub>O, or N<sub>2</sub>. The designation "M\*" indicates a higher-energy state for "M".

The initiation steps for the reaction scheme shown in Table I are probably the dissociation of H<sub>2</sub> to form H,



The dissociation of H<sub>2</sub> is shown as the reverse of reaction 6 and endothermic, requiring about 106 kcal/mole.

The concentration of H atoms is greater on the fuel-rich side of the diffusion flame. Diffusion to the oxygen-rich side provides H to form OH and H via reaction 2 or HO<sub>2</sub> via reaction 4. At low temperatures, reaction 4 is faster than

reaction 2, but  $\text{HO}_2$  concentrations will be small, less than H or OH, and  $\text{HO}_2$  is relatively unreactive compared to OH, O and H. Also, at temperatures above 870K the  $\text{HO}_2$  molecule is not present in significant concentrations due to the energy of the collision partners.<sup>21</sup> These factors suggest the contribution of  $\text{HO}_2$  to the overall mechanism is only important at low temperatures and probably small. The effects of reactions involving  $\text{HO}_2$  are stressed only in the discussion of the N/H<sub>2</sub>O mechanism.

The OH radical reactions are probably dominant because they are exothermic and the activation energy for OH reactions is very small. Table I shows that for reaction 1, the forward rate coefficient is four orders of magnitude greater than the reverse at 700K. For most of the H reactions, the reverse rate coefficients are higher or about the same as the forward coefficients. Excluding concentration effects, OH is the dominant specie in hydrogen/carbon monoxide combustion.

Chain termination in an opposed-jet diffusion flame occurs via the termolecular radical recombination reactions 6 and 7. Even though the rate coefficients for these reactions are greater than for the chain propagating reactions, the rates of the reactions are not proportionately higher because of the relatively small concentrations of H and OH.

### Oxidation Mechanism of Methane

Table II shows the complete system of methane oxidation reactions as presented by Seery and Bowman.<sup>21</sup> Approximate forward and reverse rate coefficients for these reactions were calculated at 700K and 1750K from data given by Hahn and Wendt;<sup>19</sup> Seery and Bowman did not present reverse rates or equilibrium constants. For reactions not included by Hahn and Wendt, the forward rate coefficients were taken from Seery and Bowman.

Higher temperatures allow reactions with large activation energy to become feasible, particularly the pyrolysis of methane to form methyl radical and hydrogen atom (reaction 8), and the dissociation of molecular oxygen to form oxygen atoms (reaction 10). The primary initiation step is almost certainly the pyrolysis of methane to form methyl radicals. Higher temperatures also result in large concentrations of oxygen and hydrogen atoms.

In the low temperature region of the flame edge, pyrolysis is negligible, as shown by the very small forward rate constant of reaction 8 at 700K. H atoms and OH radicals, which diffuse from the main reaction zone to the flame edge, attack  $\text{CH}_4$  via reactions 12 and 13 to form methyl radical,  $\text{CH}_3$ . The rate constants at 700K for these reactions show that they are fast at low temperature.

Methyl radical reacts with O or  $\text{O}_2$  forming formaldehyde (reactions 14 and 15). At temperatures above 1270K, reaction

15 has been ruled out on thermodynamic grounds.<sup>22</sup> The formaldehyde reaction steps, which generate product species CO and H<sub>2</sub>O are given by equations 16 and 17. At high temperatures, the decomposition of HCO (reaction 25) becomes important.

The relative contributions of reactions vary with position in the opposed-jet flame. On the fuel side of the flame, the mixture is fuel rich and contains relatively large concentrations of H atoms, deemphasizing reactions involving O and O<sub>2</sub>, and emphasizing the effects of H. As position shifts to the oxidizer side of the flame (fuel lean), OH, O and O<sub>2</sub> reactions are prominent. This is evidenced in the recorded infrared spectra as described below in the Discussion section. Fuel-rich flames generate relatively more H atoms than fuel lean flames, which generate more O and OH species.

#### Oxidation Mechanism of Ammonia

Several sources present rate constants and elementary reactions for the N/H/O system.<sup>19,20,23,24,25,26</sup> A scheme of N/H/O reactions to describe the behavior of ammonia in opposed-jet flames of methane or hydrogen/carbon monoxide and oxygen is presented in Table III with forward and reverse rate coefficients calculated at 700K and 1750K. The data used to calculate forward and reverse rate coefficients are taken from Hahn and Wendt.<sup>19</sup> Where the reverse rate coefficients are shown as N/A (not available), the reaction was not included by

Hahn and Wendt, and the forward rate coefficient was calculated from data taken from Gardiner.<sup>24</sup> The data presented by Gardiner does not include reverse rate coefficients or equilibrium constants. Reactions involving  $\text{HO}_2$  are considered separately because of the argument presented in the discussion of hydrogen/carbon monoxide oxidation, which postulates that  $\text{HO}_2$  effects may be small in opposed-jet flames.

Even though it is believed that  $\text{HO}_2$  effects are small in opposed-jet flames,  $\text{HO}_2$  has been found by Merryman and Levy<sup>27</sup> to be significant in the formation of  $\text{NO}_2$  in premixed flames. Their work also suggests that the formation of  $\text{NO}_2$  by  $\text{HO}_2$  is accompanied by formation of  $\text{OH}$ , which has a significant effect on the overall reaction rate. Therefore the contribution of  $\text{HO}_2$  reactions to N/H/O kinetics in opposed-jet flames will be examined. Table IV lists N/H/O reactions taken from Gardiner which involve  $\text{HO}_2$ . The rate coefficients for all reactions in Table IV, except reaction 49, are taken from Gardiner and are estimates with no supporting data. The values for reaction 49 are taken from Hahn and Wendt. The forward rate coefficients for reaction 49 given by Gardiner compares favorably with the value from Hahn and Wendt. Because  $\text{HO}_2$  is unstable at high temperatures, rate coefficient were calculated only at 700K.

## Inhibition Mechanisms of Specific Compounds

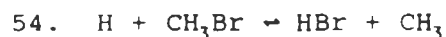
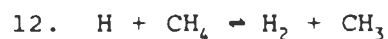
### Bromides

Friedman and Levy<sup>28</sup> evaluated the effectiveness of organic halides, which are known inhibitors, on inhibiting opposed-jet methane-air diffusion flames. They found that in the opposed-jet system organic halides rank in the order  $\text{CH}_3\text{Cl} < \text{CCl}_4 < \text{CH}_3\text{Br} \approx \text{CF}_3\text{Br}$ . This is the same ranking that has been reported for reduction of flame speed when these additives were introduced into premixed flames.<sup>29</sup> These results substantiate the validity of the opposed-jet diffusion flame method for evaluating inhibitor effects.

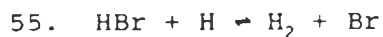
Gaydon<sup>15</sup> reviewed some of the early work on the inhibition of methane flames by halogen-containing additives. The effects are attributed to removal of OH by,



Fenimore and Jones<sup>30</sup> examined the kinetics of the reactions of methane and methyl bromide in rich, premixed hydrogen/oxygen flames. Specifically, they measured the rate of reaction 12, the attack of methane by H, and reaction 54, the attack of methyl bromide by H atom:

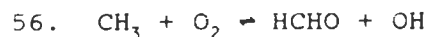


In each reaction a new free radical is formed, which is unstable but less reactive than the H atom removed, resulting in a decrease in the overall reaction rate. At 1000K and 1300K the rate of reaction 54 was found to be 100 and 20 times faster, respectively, than reaction 12. Both reactions 12 and 54 were significantly faster than reaction 8, the pyrolysis of methane. In addition, Fenimore and Jones proposed that reaction 14 for the formation of HCHO and reaction 55,



were important, further breaking the chain reaction for combustion.

Miller, Evers and Skinner<sup>31</sup> discuss the fate of methyl radicals in hydrogen flames. Reactions they propose include:



Reactions 12, 54, 55 and 57 are favored under fuel-rich conditions while reactions 14 and 56 are favored under fuel-lean conditions. In lean mixtures, active species that are removed are more likely to get back into circulation through reactions 14 and 56. This may be one reason why hydrocarbon inhibitors are less effective in lean hydrogen flames than in rich ones.

Analogous to reaction 8 is the thermal decomposition of methyl bromide:

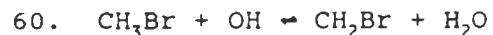


The bond dissociation energy of  $\text{CH}_3\text{-Br}$  is 70 kcal/mole versus 104 kcal/mole for  $\text{CH}_3\text{-H}$ . This results in reaction 58 becoming more feasible at lower temperatures than reaction 8, generating Br earlier in the flame than reaction 8 generates H. Thus, Br is available for inhibition through,



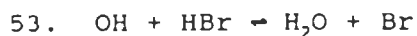
as suggested by Day, Stamp, Thompson, and Dixon-Lewis.<sup>32</sup>

Wilson<sup>33</sup> measured the temperature and composition profiles of 0.05 atm, premixed, lean methane-oxygen flames inhibited with methyl bromide and concluded that reaction 60 was the principal inhibiting reaction in that system:

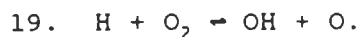


He notes that the large excess of oxygen in the system causes the hydroxyl radical concentration to far exceed the hydrogen atom concentration. This minimizes the effect of reaction 59. Wilson proposed that the flame-inhibiting mechanism was due to the inhibitor extending the preignition zone. The inhibition reactions have a lower activation energy so that radicals

which diffuse into the preignition zone react preferentially with the inhibitor. The inhibition reactions do not initiate chains so that the rate of radical generation is decreased. The reduction of the rate of generation of radicals prevents ignition from occurring until: (1) all of the inhibitor has reacted, (2) the temperature has increased until ignition occurs with a lower concentration of radicals, or (3) the concentration of radicals due to back diffusion is sufficient to overcome the reduction due to inhibition. The effect is to shift the primary reaction (measured by the maximum rate of O<sub>2</sub> consumption) to a higher temperature. The inhibited flame has a higher maximum rate and the reaction zone is compressed into a narrow region of higher average temperature. In a fuel-rich system where HBr is present in significant concentrations, reaction 53 is expected to be important:



In a later paper by Wilson, O'Donovan, and Fristrom<sup>34</sup> on the effects of HCl, HBr, and Cl<sub>2</sub>, they found that the major effect of the inhibitor was to react with H atoms, preventing the chain branching reaction,



From Day, Stamp, Thompson, and Dixon-Lewis,<sup>32</sup> Dixon-Lewis and Simpson,<sup>35</sup> and Safieh, Vandooren, and Van Tiggelin,<sup>36</sup> the

mechanism for inhibition by methyl bromide is, in addition to reactions 53, 54, and 55,



Simmons and Wolfhard<sup>37</sup> added methyl bromide to diffusion flames to determine the concentrations required for extinguishment and to study effects on flame structure. They found that the concentration required in the oxidizer to extinguish the flame was of the same order as for a premixed flame, but considerably higher concentrations were required in the fuel. When added to the air, an extra reaction zone forms on the air side in which the methyl bromide reacts, and the quenching of the flame involves an interaction of the extra zone and the main reaction zone. They also observe that the effect of adding methyl bromide to a flame can be interpreted in terms of the addition of equivalent amounts of fuel and bromine.

With the exceptions of the studies of Friedman and Levy, and Simmons and Wolfhard, all the studies cited above were performed on premixed flames.

### Ammonia

The practical importance of combustion-generated  $\text{NO}_x$  pollutants has lead to great interest in high-temperature N/H/O kinetics. Ammonia plays a significant role in the

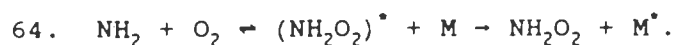
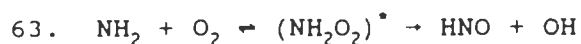
reaction schemes involving  $\text{NO}_x$  and, for example, has been used in the "thermal DeNO<sub>x</sub>" process to reduce NO concentration in flue gas.<sup>38</sup> There is considerable information regarding the reactions of ammonia in combustion system. However, in spite of the research on the kinetic mechanisms of the N/H/O system, a good deal of ambiguity still exists.

The effects of a small amount of ammonia on combustion of a fuel with oxygen depends upon the conditions of the system. The type of fuel, equivalence ratio, and concentration of species with the ability to stabilize energetic reaction products through collision determine whether ammonia will act as an inhibitor or accelerator of the combustion reactions.

It is known that ammonia inhibits ignition of dry carbon monoxide/air mixtures.<sup>39</sup> At temperatures and pressures where mixtures of carbon monoxide and air ignited without appreciable delay in a static system, addition of ammonia resulted in an induction period before explosion. However, ammonia promoted ignition outside the explosion region of the CO/air mixtures. Ammonia can also induce explosion of hydrogen/oxygen mixtures by illumination with ultraviolet light.<sup>40,41</sup> This behavior is attributed to H atoms originating from the photodissociation of  $\text{NH}_3$ .

Fujii, Miyama, Koshi, and Asaba<sup>42</sup> measured induction periods for mixtures of hydrogen, oxygen, argon, and ammonia behind reflected shock waves. They found that, for the conditions studied, the presence of ammonia significantly inhibits the chain branching reactions of the hydrogen/oxygen

system. They also found the induction period to be markedly dependent on gas composition. The mechanism they proposed for this behavior consists primarily of reactions 62, 63, and 64.

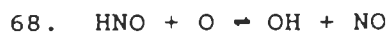
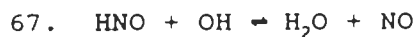


Reaction 62 is clearly inhibiting by consuming OH radicals. However, the net effect on the system depends on the fate of  $\text{NH}_2$  generated by reaction 62. If the system is rarefied and contains few species to stabilize the energetic specie  $\text{NH}_2\text{O}_2^*$  through collisional energy transfer, the result is regeneration of OH through reaction 63 and a lessening of the degree of inhibition. In the experiments of Fujii et al, this is manifested as a shorter induction period. At higher pressures and energy-removing specie concentrations, reaction 64 becomes more important and the degree of inhibition increases, resulting in longer induction periods.

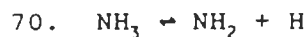
The reaction of oxygen atoms with ammonia was studied by Albers, Hoyermann, Wagner, and Wolfrum.<sup>43</sup> Besides  $\text{H}_2$ ,  $\text{H}_2\text{O}$ , NO, and  $\text{O}_2$ , they found the reaction products included HNO radicals and high concentrations of H atoms. They proposed reaction 65 as the initiating step:



Under the conditions of their measurements, the most important subsequent steps were proposed to be:



The thermal decomposition of ammonia behind shock waves was studied by Holzrichter and Wagner.<sup>44</sup> They determined the activation energy for the reaction,



to be 393 kJ/mole. The activation energy of the thermal decomposition of ammonia is so high as to make this reaction negligible in the systems studied in the work reported here.

#### Phosphorus Pentoxide

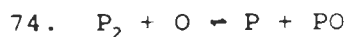
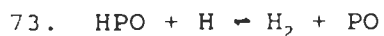
Morrison and Scheller<sup>45</sup> report the effects of trimethyl phosphate, phosphorus trichloride and phosphorus tribromide on the burning velocity of n-hexane/air flames. All of these compounds decrease the flame speed, indicating inhibition.

Triphenylphosphine oxide (TPPO) has been used as a flame retardant in nylon substrates. Mass spectrometric observations of TPPO decomposition in fuel-rich methane and

hydrogen flames have been made by Hastie.<sup>46</sup> Hastie observed  $P_2$ , PO, and  $PO_2$  with lesser amounts of P, HPO, and PN. The mechanism postulated for inhibition of flames containing TPPO begins with the decomposition of TPPO:



Radical scavenging is suggested to occur via reactions 72, 73, and 74:



Other likely reactions are:



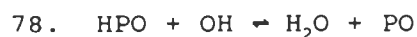
Phosphorus pentoxide,  $P_4O_{10}$ , also known as phosphoric oxide, phosphoric anhydride, or phosphoric acid anhydride, is produced by burning phosphorus in excess oxygen. The oxygen must be dry because  $P_4O_{10}$  readily reacts with water to form phosphoric acids. According to vapor density measurements, phosphorus pentoxide vapor in the temperature range of 700-1400°C consists of  $P_4O_{10}$  molecules.<sup>47</sup> There is some association below 1100°C. The structure of individual  $P_4O_{10}$

molecules in the vapor state <sup>48</sup> is shown in Figure 1. The phosphorus atoms form a regular tetrahedron. Each phosphorus atom is surrounded by a tetrahedral configuration of oxygen atoms so that each corner of the tetrahedral  $P_4O_{10}$  molecule is occupied by an oxygen atom.

The terminal oxygen atoms can be removed by reaction between  $P_4O_{10}$  and elemental phosphorus in an inert atmosphere. The electronegativity of phosphorus is 2.2, the same as hydrogen. By analogy, the terminal oxygens can be removed by H atoms, resulting in  $P_4O_x$  molecules, where x can be 9, 8, 7, or 6. These molecules retain the tetrahedral arrangement of the phosphorus atoms, but have unbonded electron pairs where the terminal oxygen atoms were removed. The removal of terminal oxygen atoms will make the molecule less stable and more reactive. Reactions with H, OH, and  $H_2O$  will become more probable, resulting in the decomposition of  $P_4O_x$  to species such as  $PO_2$ , PO, P, and HPO. Structures for phosphorous acids as shown by Pauling <sup>47</sup> suggest the reaction between  $P_4O_{10}$  and  $H_2O$  forms metaphosphoric acid,  $PO_2(OH)$ . Reaction 77 shows a likely dissociation mechanism of  $PO_2(OH)$  in the vapor phase:



Other likely reactions, in addition to those proposed by Hastie, are:



## EXPERIMENTAL APPARATUS AND METHOD

An opposed-jet burner adapted from one described by Hahn, Wendt, and Tyson<sup>6</sup> was used in conjunction with an infrared spectrometer and external optical scanning system. As shown in Figure 2, the burner consisted of two horizontal opposed tubes of circular cross section. The tubes were fitted with 304 stainless steel face plates that secured two Inconel 40-mesh wire screens per tube. Two screens were used to ensure the flatness of the screen; it was found that, upon heating, a single screen would assume a concave or convex shape resulting in a similarly curved flame. The diameter of the screened opening in the face plates was 2.5 inches. Each of the tubes was fitted with internal sleeves that secured another wire screen within the center of the tube. The space between the face screens and the internal screen was packed with 3-mm diameter glass beads while the other end of the tube was left empty. The ID of the tube sleeves was 2.125 inches and the length of each internal chamber was 3.0 inches. The sleeves contacted the face plate screens so the ID of the sleeves determined the diameter of the gas flow emerging from the burners. The gases entered the empty ends of the tubes. This arrangement was designed to develop a flat, laminar flow profile. The burner tubes were mounted on a graduated optical bench to ensure precise positioning. Spacing between the burner faces was 12 mm.

An external optical system was used to adapt a Beckman 4240 dispersive infrared spectrometer to emission measurements. The optical system is shown in Figure 3. It consisted of two 2-inch front-surface plane mirrors, a 6-inch front-surface spherical mirror of 11-inch focal length ( $f/1.8$ ) and variable slit mounted on a micrometer-adjustable translator. The variable slit and translator were positioned at the sample beam focal point of the spectrometer sample compartment. The mirrors were held in adjustable mounts on an optical bench and positioned by rod carriers. The spectrometer was operated in the single beam mode with the infrared source removed. The monochromator slit was left fully open (7-mm) and the 12-mm high variable slit was set with a 0.25 mm width and was placed at the focal point of the sample compartment. The edge-wise image of the flame was focused onto the variable slit so that the flame and its image remained fixed in space. The optics were aligned to isolate the vertical center of the flame to minimize edge effects due to buoyancy. The flame emissions were scanned from the fuel side to the oxidizer side by moving the slit across the fixed image. The image of the flame was demagnified to 75 percent of the object to provide adequate intensity for the thermopile detector of the spectrometer. The optics and burners were aligned with a laser to assure that the flame image was parallel to the slit. The optical configuration allowed scanning of the infrared emission at up to 24 adjacent

positions through the width of the flame, approximately 8 mm, from the oxidizer side to the fuel side.

The gas flow system, shown in Figure 4, was constructed from 1/4-in. copper or stainless steel tubing and Swagelok tubing fittings. Calibrated rotameters were used to control gas flow. The rotameters were calibrated with a wet test meter. Commercial grade compressed gases (hydrogen, carbon monoxide, methane, oxygen, nitrogen, and air) were used. Reagent grade additives (methyl bromide, anhydrous ammonia, and phosphorus pentoxide) were used.

Because methyl bromide and ammonia are gaseous under ambient conditions, no special equipment was required to deliver them to the flame in known concentrations; both were metered through calibrated rotameters. Methyl bromide was metered through stainless steel tubing because of its corrosive nature toward copper. Ammonia is supplied as a liquid in a pressure bottle. The latent heat of evaporation of ammonia resulted in considerable cooling of the gas to be delivered to the flame. Therefore the ammonia was heated by electrical tape wrapped around the tubing before being added to the flame to prevent erroneous results due to cooling the flame.

Phosphorus pentoxide ( $P_4O_{10}$ ), was added to the flame using an "evaporator," shown in Figure 5. Approximately 100 ppm  $P_4O_{10}$  was added to the oxygen side of each flame, which resulted in 400 ppm phosphorus atoms present in the flames. Nitrogen was used as a carrier gas to deliver  $P_4O_{10}$  to the

flame. A metered amount of nitrogen (approximately 0.1 liter per minute at ambient temperature and pressure) was passed through the heated (250°C) evaporator tube where it was assumed to become saturated with  $P_4O_{10}$ . The vapor pressure of  $P_4O_{10}$  at 250°C was calculated to be approximately 17 mm Hg.<sup>50</sup> Condensation of  $P_4O_{10}$  was prevented by heating the tubing and burner downstream from the evaporator, and by diluting the carrier gas with the heated main  $O_2/N_2$  stream at the evaporator exit. Electrical heat tapes were used to heat the evaporator, burner, and tubing.

The pressure drop across the evaporator resulted in higher pressure at the oxygen-side rotameters requiring the control flame to be operated with greater than normal back pressure to assure equal molar flow rates in both the control flame and the additive flame. A system of needle valves and a mercury manometer were used to equalize back pressure among tests. This system of valves is diagrammed in Figure 6. Referring to Figure 6, for the control flames, valves 2 and 3 were closed and valve 4 was fully open. For flames with  $P_4O_{10}$  added, valves 2 and 3 were fully open and valve 4 was closed. The pressure drop across valve 1 was varied to match the back pressure among tests.

Except for the methane/air flame documented by Tables V-VIII, all the flames were diluted with nitrogen on both sides. The mixture of hydrogen and carbon monoxide used was always a one-to-one volume ratio. The total gas flow rates used for the flames were between 24 and 34 liters per minute at ambient

temperature and pressure of nominally 72 degrees Fahrenheit and 650 millimeters of mercury. A mercury barometer and thermometer were used to keep track of conditions and rotameter calibration data was adjusted accordingly to provide accurate flow rate data. It was found that the best flame stability was achieved when the flow through each burner tube was equal at 12 to 17 liters per minute. The flow rates for each flame were tailored to result in a stable, flat flame which was well-centered between the burner faces.

The total nitrogen dilution was kept between 50 and 70 percent. The choice of fuel and overall equivalence ratio determined the amount of nitrogen added to each side, which for most cases was not equal. The procedure used to determine flow rates was a trial-and-error method. The overall equivalence ratio was chosen first, and then the amount of each gas was selected so that the equivalence ratio was achieved, the total flow was between 24 and 34 liters per minute, the flow through each burner tube was equal, and the total amount of nitrogen was between 50 and 70 percent of the total gas flow.

Before each series of tests was run, the burners were lit and allowed to operate for approximately one hour until the burners had heated up and reached thermal equilibrium. This was to prevent effects on the infrared emission due to changes in flame temperature resulting from non-equilibrium heat transfer between the flame and the burners.

## EXPERIMENTAL RESULTS

The spectral regions examined in the flames were 3800 to 2700  $\text{cm}^{-1}$  and 2450 to 2000  $\text{cm}^{-1}$ . The region 3800 to 2700  $\text{cm}^{-1}$  contains vibration-rotation bands of  $\text{H}_2\text{O}$ ,  $\text{CO}_2$ ,  $\text{OH}$ ,  $\text{CH}_4$ ,  $\text{CH}_3$ , and  $\text{HCHO}$ , and the region 2450 to 2000  $\text{cm}^{-1}$  contains bands due to  $\text{CO}_2$  and  $\text{CO}$ .<sup>51</sup> The region 2700 to 2450  $\text{cm}^{-1}$  shows only a negligible amount of continuum radiation. For methane flames a peak is recorded at 3000  $\text{cm}^{-1}$ . This peak does not occur in hydrogen/carbon monoxide flames. The position of this band suggests a C-H stretch. Species that possess bands in this region with origins at or near 3000  $\text{cm}^{-1}$  are methane, ethylene, and formaldehyde.<sup>52</sup> The concentration of ethylene in a methane flame will be negligible in comparison to methane and formaldehyde concentrations. Therefore, this peak has been assigned to methane and formaldehyde, and possibly  $\text{CH}_3$ , the relative contributions of each depending upon the position in the flame.

The bands in the 3800 to 2700  $\text{cm}^{-1}$  region show considerable broadening and overlap, especially in the center of the flame where temperatures are higher. The shapes of overlapping bands were determined by extrapolating the shape of each peak to the baseline. The frequency range covered by each band was dependent upon the height and position in the flame; bands near the center of the flame were much broader than those near the edges.

A compensating planimeter was used to measure the spectral area of the bands and the radiative intensity is taken to be directly proportional to the area. The areas are given in square inches. The error in area determinations with the planimeter depends inversely upon the size of the area being measured and is a maximum of 2 percent, but generally less, for this work. Reproducibility of the spectra for a given flame was about 2 percent. The fine structure of the flame emission spectra could not be resolved with the instrument used, but nevertheless the spectra permit evaluation of the effects of these additives.

Using a slit width of 0.25 mm, the flames were scanned in up to 24 non-overlapping intervals. The scans began at the flame edge at the fuel side and progressed to the air side of the flame. The position in the flame was recorded in inches, which was the micrometer setting of the translator that carried the variable slit; it indicates relative position only, as the location of the flame edges depended upon flow rates and overall equivalence ratio. Repeated scans of the weak emissions at the flame edges were also made. The position where the emissions just become detectable by the spectrometer used is considered to be the "extreme flame edge." It should be emphasized that the "flame edge" is determined by the sensitivity of the detector and does not necessarily relate to the kinetics of the flame.

Additive concentrations were calculated as a percentage of the total volume of gases flowing through both burner tubes

unless noted otherwise. Local concentrations in the opposed-jet flame were not determined. In order to isolate the effects of bromine, the rate of fuel flow in the tests reported here was corrected for the fuel value of the methyl bromide.

The effects of all three additives, methyl bromide, phosphorus pentoxide, and anhydrous ammonia, were investigated in flames of methane and a one-to-one mixture of hydrogen and carbon monoxide. Both fuels were oxidized with oxygen, and nitrogen was used as a diluent. Fuel-rich, stoichiometric, and fuel-lean flames were used. The overall equivalence ratio was varied between 0.5 and 2.0. Methyl bromide was added to either the fuel side or the oxygen side of the burners; phosphorus pentoxide and anhydrous ammonia were added only to the oxygen side.

#### Methyl Bromide

Typical spectra for an undiluted methane-air flame with methyl bromide added to the air side are shown in Figures 7a, 7b, and 7c, for the fuel side, the middle, and the air side of the flame, respectively. The overall equivalence ratio was 0.86. On the air side, Figure 7c, only the  $\text{H}_2\text{O}/\text{OH}/\text{CO}_2$  bands, 3700 to 3000  $\text{cm}^{-1}$ , and the  $\text{CO}_2/\text{CO}$  band, 2400 to 2000  $\text{cm}^{-1}$  are visible. Further into the flame, Figure 7b,  $\text{HCHO}/\text{CH}_4$  band is quite evident centered at 3000  $\text{cm}^{-1}$ . Finally, on the fuel side of the flame, there is seen a composite of  $\text{H}_2\text{O}$ ,  $\text{OH}$ ,  $\text{CH}_4$ ,  $\text{HCHO}$ ,

and probably  $\text{CH}_3$  band spectra. These characteristic bands are also found in the flame without methyl bromide, but the intensity of all the bands in the main reaction zone is enhanced when methyl bromide is added.

The data in Tables V-VIII were taken on a flame of undiluted methane oxidized with air. Methyl bromide was added to the air side of the flame at a level of 1.6 percent of the total fuel flow. The overall equivalence ratio for this flame was 0.86. Table V summarizes the areas obtained from the emission spectra for the 3700 to 2700  $\text{cm}^{-1}$  region as a function of position in the flame with and without methyl bromide. Table VI contains the corresponding areas for the spectral region 2450 to 2000  $\text{cm}^{-1}$ . Figures 8 and 9 display the data listed in Tables V and VI, respectively. The fuel side of the flame is at slit position 0.00 inch and the air side is at 0.24 inch. The areas under the bands centered at 3470  $\text{cm}^{-1}$  (mostly  $\text{H}_2\text{O}$  and OH) and 3000  $\text{cm}^{-1}$  (HCHO,  $\text{CH}_2$  and possibly  $\text{CH}_3$ ) were separated from the total area of the region 3700 to 2700  $\text{cm}^{-1}$  in order to further define the effects of methyl bromide. These data are listed in Tables VII and VIII, and displayed in Figures 10 and 11.

The data in Tables V and VI and Figures 8 and 9 show that the intensity of emissions on the flame edges, particularly on the fuel side, is decreased. This indicates that the reactions at the flame edges are suppressed. Within the reaction zone, however, all the spectra in the regions recorded are enhanced by the addition of methyl bromide. The

enhancement is greater on the air side of the flame. It will be noted that the percentage increase in intensity of the band at  $3000\text{ cm}^{-1}$ , which is interpreted as predominantly HCHO, (except nearer the fuel-side flame edge where  $\text{CH}_4$  and probably  $\text{CH}_3$  spectra are present) is much greater than for the  $3470\text{ cm}^{-1}$  band for  $\text{H}_2\text{O/OH}$ . The  $3000\text{ cm}^{-1}$  emission of fuel and intermediate species, HCHO/ $\text{CH}_4$ / $\text{CH}_3$ , falls to zero at the position 0.15 inch where the emissions for product species  $\text{CO}_2/\text{CO}$  and  $\text{H}_2\text{O/OH}$  are at a maximum. This relationship is shown in Figure 12. This lends further credibility to the assignment of the  $3000\text{ cm}^{-1}$  band to HCHO/ $\text{CH}_4$ / $\text{CH}_3$ .

A study was conducted at the extreme edges of a fuel-rich, methane-oxygen flame ( $\phi=2.0$ ) with and without 0.6% methyl bromide added to the fuel side of the flame. Both methane and oxygen were diluted with nitrogen. The slit was positioned at each edge such that the intensity of  $\text{CO}_2/\text{CO}$  emission in the  $2400$  to  $2000\text{ cm}^{-1}$  region was near the limit of detectability for the spectrometer. At these points there was no detectable emission in the  $3700$  to  $2700\text{ cm}^{-1}$  region. On each side of the flame ten scans at the same position were taken without methyl bromide and ten scans with methyl bromide. The results, shown in Table IX, show that the amount of  $\text{CO}_2/\text{CO}$  at the edges decreases upon addition of methyl bromide indicating extension of the preignition zone due to inhibition.

Methyl bromide was also added to a number of hydrogen/carbon monoxide flames. These results are presented in Tables X-XVII.

Tables X-XIII summarize the data collected on the effects of methyl bromide addition to hydrogen/carbon monoxide flames of overall equivalence ratio of 0.86. These data were taken to provide a comparison to the methane flame of the same equivalence ratio. Table X lists the spectral areas of the 3800 to 2900  $\text{cm}^{-1}$  ( $\text{H}_2\text{O}/\text{OH}/\text{CO}_2$ ) emission with and without 3.0 percent methyl bromide added to the oxygen side of the flame, and Table XI lists the spectral areas for the 2450 to 2000  $\text{cm}^{-1}$  ( $\text{CO}_2/\text{CO}$ ) emission for the same flame. Methyl bromide was also added to the fuel side of the  $\phi=0.86$  flame at 0.6 percent. For this flame, the areas for the 3800 to 2900  $\text{cm}^{-1}$  region are listed in Table XII, and the 2450 to 2000  $\text{cm}^{-1}$  areas are given in Table XIII.

The data in Tables X-XIII show that the effect of methyl bromide is greater on the 3800 to 2900  $\text{cm}^{-1}$  emission, which is predominantly  $\text{H}_2\text{O}$ , than on the 2450 to 2000  $\text{cm}^{-1}$  band, which is solely due to  $\text{CO}_2/\text{CO}$  emission. In comparison with the other data presented in this work, Table XII shows a higher degree of inhibition; the emissions are suppressed much farther into the main flame zone than any other flame, and the increase in emission from the flame center is small.

Tables XIV-XVI summarize data taken on hydrogen/carbon monoxide flames with overall equivalence ratios of 0.5 and 1.0. These flames were scanned from edge to edge with a 0.25

mm slit width, but only seven segments were scanned, which were not immediately adjacent to one another, but evenly spaced through the width of the flames. Table XIV lists emission measurements for the 3800 to 2700  $\text{cm}^{-1}$  and 2450 to 2000  $\text{cm}^{-1}$  regions for a  $\phi=0.5$  flame with 0.2 percent methyl bromide added to the fuel side. Table XV presents data for a  $\phi=0.5$  flame where a comparison was made between 0.2 percent methyl bromide added to fuel side of the flame versus 0.2 percent methyl bromide added to the oxygen side. Table XVI shows the results of adding 0.2 percent methyl bromide to the oxygen side of a  $\phi=1.0$  (stoichiometric) flame. For the flames documented by Tables XV and XVI, only the emissions in the 2450 to 2000  $\text{cm}^{-1}$  region were recorded.

The behavior of hydrogen/carbon monoxide flame emissions upon methyl bromide addition is essentially the same as methane flames; the intensity of emissions increases at the flame center and decreases at the flame edges showing that the preignition zones are extended and the main reaction zones are narrowed and increased in temperature with inhibition. The total increase in emission of hydrogen/carbon monoxide flames upon addition of methyl bromide is less than for methane flames. The difference is that the 3000  $\text{cm}^{-1}$  band in methane flames shows a very large increase. If a comparison is made between methane flames and hydrogen/carbon monoxide flames excluding the 3000  $\text{cm}^{-1}$  band in methane flames, the total increase in emissions for the two fuels is approximately the same.

### Ammonia

Anhydrous ammonia was added to the oxygen side of methane flames and hydrogen/carbon monoxide flames. The amount of ammonia added was 0.21 percent for all the flames studied. Overall equivalence ratios of 0.5, 1.0 and 2.0 were used for methane flames; for hydrogen/carbon monoxide flames only  $\phi=1.0$  was used.

The results of ammonia addition to  $\phi=2.0$  and  $\phi=0.5$  (fuel-rich and fuel-lean, respectively) methane flames are shown in Tables XVII and XVIII. For both flames the 2450 to 2000  $\text{cm}^{-1}$  region was scanned at two points in the flame; one point on the fuel-side of center and one on the oxygen-side of center. The points scanned were well into the main reaction zone and about one-third the height of the maximum intensity recorded for this flame. The results show that the emission of the  $\text{CO}_2/\text{CO}$  band from the main reaction zone increases slightly upon ammonia addition and that this behavior is independent of overall equivalence ratio within the range studied.

The results of ammonia addition to a methane flame of  $\phi=1.0$  are presented in Table XIX. The flame used to generate the data shown in Table XIX was scanned at four points between the fuel side and mid-flame; the emission from the oxygen side of center was not recorded. Table XIX lists the spectral areas from the regions 2450 to 2000  $\text{cm}^{-1}$  and 3800 to 3050  $\text{cm}^{-1}$ , and the area of the peak centered at 3000  $\text{cm}^{-1}$ . Examination of the data presented in Table XIX shows that the  $\text{CO}_2/\text{CO}$

emission in the 2450 to 2000  $\text{cm}^{-1}$  range increases in intensity on the fuel-side of the flame but is not affected near the center. The region 3800 to 3020  $\text{cm}^{-1}$  shows a decrease at the fuel-side edge of the flame and an increase at mid-flame. The 3800 to 3020  $\text{cm}^{-1}$  regions manifests two bands which are normally overlapping. At one position in the flame these bands can be separated into two bands covering the regions 3800 to 3300  $\text{cm}^{-1}$  and 3300 to 3020  $\text{cm}^{-1}$ . The 3300 to 3020  $\text{cm}^{-1}$  band emission decreases in intensity upon ammonia addition while the 3800 to 3300  $\text{cm}^{-1}$  band emission is virtually unchanged. At the extreme fuel-side of the flame, emission from the 3800 to 3020  $\text{cm}^{-1}$  region was too small to be integrated with the planimeter, but it was obvious that the intensity was decreased upon ammonia addition. The emission of the HCHO/CH<sub>4</sub>/CH<sub>3</sub> band increased in intensity and persisted farther into the flame towards the oxygen side upon addition of ammonia.

Repeated scans at the extreme oxygen-side and fuel-side flame edges with and without ammonia were performed on methane flames of  $\phi=1.0$ . The results of these scans are presented in Tables XX and XXI. The flames scanned to generate the data in Tables XX and XXI were both of  $\phi=1.0$ , but were of slightly different flow rates. Examination of Table XX shows that upon ammonia addition, the intensity of CO<sub>2</sub>/CO emission in the 2350 to 2200  $\text{cm}^{-1}$  region decreases on the fuel-side edge of the flame and increases on the oxygen-side edge. Table XXI shows similar behavior with the oxygen-side edge 3600 to 3000  $\text{cm}^{-1}$

emission increasing and the fuel-side edge 2350 to 2200  $\text{cm}^{-1}$  emission decreasing. Emission from the 2350 to 2200  $\text{cm}^{-1}$  region was too weak to be recorded at the point scanned on the oxygen side of the flame.

Ammonia was also added to a stoichiometric hydrogen/carbon monoxide flame. Repeated scans were made at two points on the oxygen side of the flame; the first point was in the main reaction zone where the peak intensity was about one-third the maximum, and the second was at the edge of the flame. The regions 2400 to 2100  $\text{cm}^{-1}$  and 3800 to 3100  $\text{cm}^{-1}$  were scanned at the first point. Only the 2400 to 2100  $\text{cm}^{-1}$  region was scanned at the second point because at the edge of the flame no emission from the 3800 to 3100  $\text{cm}^{-1}$  was detectable. Table XXII lists the data taken at the first point in this flame and Table XXIII lists the data taken at the second point in the flame. The behavior of hydrogen/carbon monoxide flames upon ammonia addition is seen to be similar to the behavior of methane flames in that the emission from the main reaction zone increases and the emission at the extreme flame edges decreases indicating extension of the preignition zone while the main reaction zone becomes narrower and increases in temperature.

#### Phosphorus Pentoxide

Phosphorus pentoxide was added to fuel-rich ( $\phi=2.0$ ) and fuel-lean ( $\phi=0.5$ ) hydrogen/carbon monoxide flames, and a

stoichiometric ( $\phi=1.0$ ) methane flame. Tables XXIV and XXV show the results of phosphorus pentoxide addition on hydrogen/carbon monoxide flames of  $\phi=2.0$  and  $\phi=0.5$ , respectively. Figures 12 and 13 present the data listed in Table XXV. The  $H_2/CO$  flames were scanned from edge to edge with a 0.25 mm slit width, but only seven, evenly spaced segments were scanned.

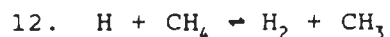
Table XXVI shows the effects of  $P_4O_{10}$  addition on the emissions from the edges of a stoichiometric methane flame; only the extreme edges of the methane flame were scanned. Five to eight scans at the same position were averaged to generate each data point in Table XXVI.

The data in Tables XXIV, XXV, and XXVI and Figures 12 and 13 show that, for all the flames tested, the addition of phosphorus pentoxide results in an increase in emission intensity of the spectral regions measured across the entire width of each flame. The data also show that the emission intensity increases at the extreme flame edges indicating a broadening of the flame. Also, a bright, white, visible emission was observed in flames containing  $P_4O_{10}$ .

## DISCUSSION

Methyl Bromide

The measured spectra support the mechanism for combustion of methane via the reactions,



and the subsequent reactions shown in Table II above. It is unlikely that methyl bromide added on the air side could pass through the main reaction zone intact. Pyrolysis of  $\text{CH}_3\text{Br}$  to  $\text{CH}_3$  and Br on the fuel-lean, oxygen side of the flame can produce Br atoms to diffuse to the fuel side where reaction with H atoms forming HBr by reaction 59 can occur. Reaction 59 removes the chain carrying specie H and forms HBr, which subsequently reacts with H and OH (reactions 53 and 55) forming the stable reactant or product species  $\text{H}_2$  or  $\text{H}_2\text{O}$ , while removing reactive chain carrying species H or OH, and regenerating the inhibitor, Br. Diffusion of Br and HBr to the fuel side of the flame where they engage in the regenerative cycle of reactions 53, 55, and 59 results in a reduction of the free radical concentrations and a consequent extension of the preignition zone.

Inhibition of the flame can also occur by the reaction of  $\text{CH}_3\text{Br}$  with OH by reaction 61 to form HCHO and HBr. HCHO then reacts with OH to form  $\text{H}_2\text{O}$  and HCO, which is less reactive than the OH radical removed. The HBr formed can engage in the inhibition cycle of reactions 53, 55, and 59 described above. The reaction of methyl bromide with OH and the back-diffusion of Br and HBr to the air side of the flame results in extension of the preignition zone on the air side.

Inhibition and the resultant extension of preignition zones are evidenced by the reduced spectral areas recorded at the flame edges and shown in Tables V-VIII and Figures 7-10. In particular, the reduction of the spectral area at the flame edges of the region 2400 to 2000  $\text{cm}^{-1}$ , where the only emitters are CO and  $\text{CO}_2$ , demonstrates the inhibition of the formation of CO and  $\text{CO}_2$ . Since all reactions in the above scheme given for combustion of methane which result in the formation of CO and  $\text{CO}_2$  involve the OH radical, these results support the proposed inhibition reactions 53, 60 and 61, which consume OH. Also, because of the unlikeliness of methyl bromide passing through the flame intact and the observation of inhibition on both sides of the flame, the presence of HBr (required by reactions 53 and 55) is substantiated and reactions 54, 58 and 59, which form HBr, are supported. The presence of HBr having been established, reaction 55 is also supported.

The increase in the  $\text{HCHO}/\text{CH}_4/\text{CH}_3$  emission at 3000  $\text{cm}^{-1}$  upon methyl bromide addition can also be explained by the lowered H and OH concentration. This results in slowing the

rate of  $\text{CH}_4$ ,  $\text{CH}_3$  and  $\text{HCHO}$  consumption thus increasing their concentrations at fuel-side points in the flame. Reduction of  $\text{OH}$  concentration results in inhibition of further reaction of  $\text{HCHO}$  by reaction 16, and lowered  $\text{H}$  and  $\text{OH}$  concentrations reduces the rate of the methane-consuming reactions 12 and 13. Figure 11 shows that the  $\text{HCHO}/\text{CH}_4/\text{CH}_3$  band at  $3000\text{ cm}^{-1}$  extends further into the main reaction zone, toward the oxygen side of the flame, upon methyl bromide addition. This is probably due to a combination of increased temperature and delayed consumption of  $\text{CH}_4$ ,  $\text{HCHO}$ , and  $\text{CH}_3$  because of inhibition.

The mechanism by which methyl bromide inhibits flames of hydrogen/carbon monoxide is expected to be very similar to the mechanism of inhibition of methane flames. With the exception of the discussion of the  $\text{HCHO}/\text{CH}_4/\text{CH}_3$  emission, the above discussion regarding the inhibition mechanisms of methyl bromide in methane flames applies to hydrogen/carbon monoxide flames.

Since the amount of methyl bromide added to the flames was not sufficient to quench combustion completely, the inhibition effects were predominantly at the flame edges. One result of the partial inhibition, as observed by Wilson,<sup>33</sup> was to narrow the main reaction zone and to increase the average temperature. This resulted in the increase in emission recorded for the spectra studied.

The  $\text{H}_2\text{O}/\text{CO}_2/\text{CO}$  emission intensity curves shown in Figures 8 and 9 show an anomalous increase on the oxygen side of the flame with methyl bromide added to the oxygen side. This

increase may be the result of the extra reaction zone observed by Simmons and Wolfhard.<sup>37</sup> Also, the observation of Simmons and Wolfhard that methyl bromide is more effective when added to the oxygen side of a diffusion flame than when added to the fuel side is corroborated by the results presented in Table XV. These results show that, upon methyl bromide addition, the percent increase in  $\text{CO}_2/\text{CO}$  emission is greater when methyl bromide is added to the oxygen side of the flame.

### Ammonia

The experimental data indicate that ammonia added to the oxygen side of opposed-jet diffusion flames acts to inhibit combustion reactions on the fuel-side of the flame and accelerates combustion on the oxygen-side of the flame.

The data presented in Tables XVII, XVIII, and XIX show that ammonia affects methane flame emissions from the fuel side in the same manner as methyl bromide, i.e., the emission intensity from the main reaction zone is increased, the intensity at the extreme fuel-side edge is decreased, and the emission of the  $\text{HCHO}/\text{CH}_2/\text{CH}_3$  band at  $3000\text{ cm}^{-1}$  is increased and extends farther into the flame towards the oxygen side. This indicates that inhibition is occurring on the fuel-side of the flame when ammonia is added. However, Tables XVII, XVIII, and XIX do not record the effects on the oxygen side of the flame. Tables XX and XXI present data collected on the extreme edges of methane flames and show that, upon ammonia addition,

emission intensity is significantly increased on the oxygen side and decreased on the fuel side. The increased emission on the oxygen side indicates that ammonia accelerates the combustion reactions on the oxygen side of the flames. Evaluation of the data presented in Tables XXII and XXIII shows that ammonia affects hydrogen/carbon monoxide flames in the same way it affects methane flames.

A mechanistic explanation of the effects of ammonia on opposed-jet diffusion flames can be drawn from the reaction schemes and rate constants presented in Tables I-IV above.

The following argument can explain the acceleration of oxygen-side combustion by ammonia. On the oxygen side, the dominant free radicals are O and OH. The hydroperoxy radical, HO<sub>2</sub> may also be present, as discussed above in the section on Oxidation Mechanism of Hydrogen/Carbon Monoxide. The reactions on NH<sub>x</sub> species with OH are given by equations 29, 33, 37, and 38. Reactions 29, 33, and 38 produce NH<sub>x-1</sub> and water. Reaction 37 produces HNO and H atoms. Reactions of NH<sub>x</sub> with O are given by equations 28, 31, 32, 35, and 36. The reactions of NH<sub>x</sub> with O all form either H atoms or OH radicals, both of which are more reactive than O. Reactions of HNO, which is formed by reactions 32 and 37, with O and OH are shown by equations 40 and 41. Reaction 41 forms OH radicals. The NH<sub>x</sub> reactions with O are chain propagating because they result in no net change in the number of chain carriers. They can be considered accelerating because the chain carrier generated by the reactions (OH) is more reactive

than the one consumed (O). Also, the reaction rate coefficients of  $\text{NH}_x$  with O or OH are as large or larger than the corresponding coefficients for O and OH reactions in the hydrogen/carbon monoxide or methane systems making the  $\text{NH}_x$  reactions competitive or, in some cases, dominant. If one includes the effects of  $\text{NH}_x$  reactions with  $\text{HO}_2$ , the argument for acceleration on the oxygen side still holds. Reactions 42 and 44 produce  $\text{H}_2\text{O}_2$  which can dissociate into two OH radicals. These are chain branching steps. However, the forward rate coefficient of reaction 42 is eight orders of magnitude smaller than for reaction 44, making reaction 42 negligible. The rate coefficient for reaction 44 is large and comparable to the fastest reactions in the systems considered. Thus the inclusion of  $\text{HO}_2$  reactions, the importance of which have been questioned, does not invalidate the argument for acceleration of oxygen-rich combustion by ammonia.

The inhibition of combustion on the fuel side by ammonia follows a similar argument. The dominant free radicals on the fuel side are OH and H atoms. Reactions of  $\text{NH}_x$  with H are given by equations 27 and 30. The reaction products of reactions 27 and 30 are  $\text{NH}_{x-1}$  and  $\text{H}_2$ . This behavior makes them inhibiting reactions because they remove chain carriers and generate the stable specie,  $\text{H}_2$ . The reactions of  $\text{NH}_x$  with OH (reactions 29, 33, 37, and 38) are also inhibiting, removing OH to generate  $\text{NH}_{x-1}$  and the stable product specie,  $\text{H}_2\text{O}$ . Reaction 37 generates HNO and H atom making it a chain propagating reaction, but HNO inhibits the system by reacting

with OH via reaction 40 to remove OH radicals and generate H<sub>2</sub>O. The reactions of NH<sub>x</sub> with HO<sub>2</sub> do not apply on the fuel side of the flame because HO<sub>2</sub> radicals are produced on the oxygen side and cannot survive the high temperatures encountered while diffusing to the fuel side. The reaction rate coefficients of NH<sub>x</sub> reactions with H and OH are as large or larger than the corresponding rate coefficients in the hydrogen/carbon monoxide or methane systems making the inhibiting NH<sub>x</sub> reactions competitive.

The mechanisms shown in Tables I-IV do not include the interactions between hydrocarbon fragments CH<sub>x</sub> and the oxidation products of ammonia such as HNO, NO, N, and NH to form species such as CN and HCN. The species involved in these reactions occur in the high temperature main reaction zone and have very small concentrations in the low temperature regions of the extreme flame edges. Since inhibition occurs in the early stages of the flame, this work is not concerned with the reactions of species occurring predominantly in the advanced stages of the flame.

#### Phosphorus Pentoxide

The experimental data show that, upon P<sub>4</sub>O<sub>10</sub> addition, the infrared emission intensity increases across the entire width of the flames studied, and that the width of the flames, as measured by infrared emission, increases. Given the experimental parameters, these results cannot be easily

explained within the bounds of the assumptions of chemical and thermal equilibrium, and constant self-absorption.

The proposed decomposition mechanism for  $P_4O_{10}$  generates the same species as the mechanisms proposed by Hastie for inhibition by TPPO. The  $P_4O_{10}$  decomposition mechanism is supported by the observation of a visible glow in flames with  $P_4O_{10}$ . The glow is attributed to emission of HPO and PO.<sup>53</sup> This supports the position that  $P_4O_{10}$  should act as an inhibitor. A possible explanation of the experimental results is that inhibiting reactions are occurring in the "dark" preflame region where emissions are below the detection threshold of the spectrometer. This is unlikely because  $P_4O_{10}$  is a stable molecule and its decomposition at low temperatures should be slow. Also, the methyl bromide results show inhibition occurring in the region detectable with this equipment, decreasing the likelihood of significant reactions occurring in the "dark" preflame zone.

Since  $P_4O_{10}$  has no fuel value, and probably undergoes endothermic decomposition, the observed effect cannot be due to additional energy being introduced into the system via  $P_4O_{10}$ .

The heating effect of the carrier gas is negligible because the amount of carrier gas was small, less than one-half percent of the total gas flow. Also, the main  $O_2/N_2$  stream was heated, so the temperature difference between the carrier gas and the main stream was small.

Pressure differences in the gas delivery system between control flames and additive flames would result in an overall increase in the oxygen delivered to the flame, which could result in the observed behavior. However, this problem was anticipated and the test apparatus and method were designed to prevent its occurrence.

The presence of  $P_4O_{10}$  may also lower the degree of ionization or dissociation occurring in the flame, which would result in higher temperatures. This mechanism cannot explain the increased radiation from the flame edges, because temperatures at the edges are too low for significant dissociation or ionization.

The decomposition products of  $P_4O_{10}$  include HPO and PO, which have infrared active vibration-rotation transitions. The frequencies of these bands were not found in the literature and their calculation is beyond the scope of this study. Therefore, the contributions of HPO and PO to infrared emissions in the regions studied could not be determined.

It is concluded that the most likely explanation for the observed behavior of  $P_4O_{10}$ -doped flames is deviation from equilibrium conditions. Phosphorus is the classical example of chemiluminescence, i.e., phosphorescence. The formation of molecules with excess vibrational-rotational energy, particularly  $CO_2$ , CO and OH, is known to occur in flames<sup>54</sup>, and the nature of phosphorus with its forbidden transitions may prolong the relaxation time resulting in a deviation from thermal equilibrium and the potential for an increase in

emission from  $P_4O_{10}$ -doped flames. The possibility of formation of non-phosphorus species in an excited state through  $P_4O_{10}$  decomposition reactions also exists. The resulting deviation from equipartition of energy would increase the infrared radiation. The decomposition of  $P_4O_{10}$  in the flame may also delay reaching chemical equilibrium, resulting in elevated concentrations of OH and CO and a subsequent increase in radiation.

#### Applications to Solid Propulsion

The additives studied here exhibit chemistry which would suppress rocket exhaust afterburning. However, their direct use in practical propulsion systems is not likely.

To be useful in solid propulsion systems, additives must meet a number of requirements in addition to being effective inhibitors. They must be chemically stable and chemically compatible with other propellant ingredients. They cannot have adverse effects on the propellant burning rate and pressure exponent. Also, additives used for afterburning suppression ideally should not increase other signatures of the exhaust plume such as smoke, radar cross section, and visible light emission.

The methyl bromide tests indicate that brominated compounds inhibit afterburning. But the formation of HBr in the plume would increase the propensity for contrail formation, decreasing the desirability of bromine for use in

solid propulsion. The effects of small amounts of HBr on smoke formation should be investigated. It is possible that the small amounts required for afterburning suppression will not have a significant impact on smoke formation. Several ways of incorporating bromine in solid propellants exist. The polymers used for fuel and binder could be brominated, and bromide salts such as ammonium bromide might be compatible. In the case of bromide salts, the cation must be chosen such that the bond energy of the salt is sufficiently low to allow low temperature dissociation.

Ammoniacal compounds have also been shown to inhibit combustion when introduced to the fuel side of a diffusion flame; in a rocket exhaust, the suppression additive is introduced on the fuel side of the flame making ammoniacal compounds chemically appropriate as an inhibitor. The use of ammonium bromide could possibly result in inhibition by both bromine and ammonia.

The use of phosphorus compounds is probably unacceptable because of the bright, visible emission of hot  $\text{HPO}$  and  $\text{PO}$ , which would occur even in the absence of afterburning.

## CONCLUSIONS

### Methyl Bromide

This work corroborates the conclusion of Friedman and Levy<sup>28</sup> that the opposed-jet diffusion flame is a valid tool for studying inhibition of combustion by chemical additives.

Wilson's<sup>33</sup> observation of methyl bromide addition extending the preignition zone, narrowing the main reaction zone, and increasing the average temperature were confirmed.

The emission intensity increase and spatial shift of the  $3000\text{ cm}^{-1}$  HCHO/CH<sub>4</sub> peak upon methyl bromide addition confirms inhibition and reinforces the importance of HCHO in the mechanism of hydrocarbon oxidation.

The observations of Simmons and Wolfhard<sup>37</sup> regarding the formation of an additional reaction zone when methyl bromide is added to the oxygen side of a diffusion flame were corroborated. This work also corroborates the observation of Simmons and Wolfhard that the effects of methyl bromide are greater when added to the oxygen side of a diffusion flame than when added to the fuel side.

These results also support the mechanisms proposed by Fenimore and Jones<sup>30</sup>, and by Wilson<sup>33</sup> for the reactions of CH<sub>3</sub>Br with H and HBr with OH in breaking the chain reactions required for the combustion.

It was not possible by examining the infrared emissions of opposed-jet diffusion flames to identify with certainty

which specific reactions dominate the inhibition of combustion of methane or hydrogen/carbon monoxide by methyl bromide. It is likely that, in the opposed-jet system, all of the inhibition mechanisms discussed above are occurring in the flame. The degree of contribution of one mechanism or another depends upon the location in the diffusion flame and overall equivalence ratio.

#### Ammonia

Ammonia can act as either an inhibitor or accelerator of combustion reactions. In fuel rich systems, it behaves as an inhibitor by removing H atoms and OH radicals to form  $H_2$  and  $H_2O$ , respectively. In oxygen rich systems it behaves as an accelerator by reacting with O atoms in chain propagating steps to generate OH radicals, which are more reactive than O atoms. Including  $HO_2$  reactions, there is a chain branching reaction resulting in the formation of two OH radicals for each O atom consumed.

#### Phosphorus Pentoxide

Phosphorus compounds are known to be inhibitors of combustion reactions. However, the effect of  $P_4O_{10}$  on the reaction rate of opposed-jet diffusion flames cannot be determined from the present experimental results. The results show an increase in flame width and emission intensity, which

conflict with the principles of flame thermochemical dynamics based on assumptions of chemical and thermal equilibrium. The most likely explanation for these results is deviation from thermal and/or chemical equilibrium induced by the presence of  $P_4O_{10}$  in the flame. The specific mechanism responsible for this behavior could not be identified.

#### Applications to Solid Propulsion

The direct use of the additives studied here in practical solid propulsion systems is not likely. Derivatives of ammonia and bromine have promise and further investigation is recommended.

## REFERENCES

1. R.C. Oliver, "Smokeless Solid Propellants: an Overview," Institute for Defense Analysis, Arlington, Va., Report IDA RP 472, March, 1969.
2. H.E. Scott, "Tactical Missile Signatures Under Wind Tunnel Simulated Conditions," Arnold Engineering Development Center, Report No. AEDC-TR-80-13, 1982.
3. E. Miller, "Smokeless Propellants," Fundamentals of Solid Propellant Combustion: AIAA Progress in Astronautics and Aeronautics, Vol. 90, edited by K.K. Kuo, AIAA, New York, New York, 1984, pp 841-884.
4. E.T. McHale, "Chemical Interpretation of Suppression of Missile Plume Afterburning by Chemical Agents," 9th JANNAF Plume Technology Meeting, Kennedy Space Center, Florida, 4-6 February, 1976.
5. Engineering Design Handbook. Spectral Characteristics of Muzzle Flash, Army Materiel Command Pamphlet No. 706-255 (1967).
6. D.E. Jensen and G.A. Jones, "Theoretical Aspects of Secondary Combustion in Rocket Exhausts," Combustion and Flame **41**, pp 71-85 (1981).
7. W.A. Hahn, J.O. Wendt, and T.J. Tyson, "Analysis of the Flat Laminar Opposed-Jet Diffusion Flame with Finite Rate Detailed Chemical Kinetics," Combustion Science and Technology **27**, pp 1-17 (1981).
8. P.G. Ashmore, "Elementary Combustion Reactions. Neutral Species," Tenth Symposium (International) on Combustion, The Combustion Institute, pp 377-386 (1965).
9. I. Glassman, Combustion, Academic Press, New York, New York, 1977, p 33.
10. I. Glassman, Ibid., p 19.
11. I. Glassman, Ibid., p 20.
12. E.M. Bulewicz and T.M. Sugden, "The Recombination of Hydrogen Atoms and Hydroxyl Radicals in Hydrogen Flame Gases," Trans Faraday Soc. II, pp 1855-1860 (1958).

13. D.E. Jensen and G.A. Jones, " Reaction Rate Coefficients for Flame Calculations," Combustion and Flame 32, pp 1-34 (1978).
14. T.M. Sugden, "Elementary Combustion Reactions. Charged Species," Tenth Symposium (International) on Combustion, The Combustion Institute, pp 539-544 (1965).
15. A.G. Gaydon, The Spectroscopy of Flames, 2nd Edition, John Wiley and Sons, Inc., New York, New York, 1974.
16. C.C. Ferriso, "The Emission of Hot CO<sub>2</sub> and H<sub>2</sub>O in Small Rocket-Exit Exhaust Gases," Eighth Symposium (International) on Combustion, The Combustion Institute, pp 275-287 (1960).
17. A.G. Gaydon, Ibid., p 228.
18. I. Glassman, Ibid., pp 1-15.
19. W.A. Hahn and J.O.L. Wendt, "NO<sub>x</sub> Formation in Flat, Laminar, Opposed Jet Methane Diffusion Flames," Eighteenth Symposium (International) on Combustion, The Combustion Institute, p 121 (1981).
20. J.M. Levy, J.L. Longwell, A.F. Sarofim, T.L. Corley, M. Heap, and T.J. Tyson, "NO<sub>x</sub> Abatement in Fossil Fuel Combustion:Chemical Kinetic Considerations," Proc. of the Third Stationary Source Combustion Symposium, Vol. 4 Fundamental Combustion Research and Environmental Assessment, Interagency Energy/Env. Res. and Dév. Prog., Report No. EPA-600/7-79/050d, February, 1979.
21. D. Seery and C.T. Bowman, Combustion and Flame 14, p 37 (1970).
22. S.W. Benson, National Bureau of Standards Spec. Publ. 357, p 121 (1972).
23. T.M. Sloane (Ed.), The Chemistry of Combustion Processes, ACS Symposium Series Vol. 249, American Chemical Society, 1984, pp 71-86.
24. W.C. Gardiner, Jr. (Ed.), Combustion Chemistry, Springer-Verlag New York Inc., New York, New York, pp 361-421 (1984).

25. T. Takagi, T. Tatsumi, and M. Ogasawara, "Nitric Oxide Formation From Fuel Nitrogen in Staged Combustion: Roles of HCN and  $\text{NH}_3$ ," Combustion and Flame **35**, pp 17-25 (1979).
26. S. Salimian, R.K. Hanson, and C.H. Kruger, "Ammonia Oxidation in Shock-Heated  $\text{NH}_3$ - $\text{N}_2\text{O}$ -Ar Mixtures," Combustion and Flame **56**, pp 83-95 (1984).
27. E.L. Merryman and A. Levy, Fifteenth Symposium (International) on Combustion, The Combustion Institute, p 1073 (1974).
28. R. Friedman and J.B. Levy, "Inhibition of Opposed-jet Methane-Air Diffusion Flames. The Effects of Alkali Metal Vapours and Organic Halides," Combustion and Flame **7**, pp 195-201 (1963).
29. W.A. Rosser, Jr., H. Wise, and J. Miller, Seventh Symposium (International) on Combustion, The Combustion Institute, pp 175-182 (1959).
30. C.P. Fenimore and G.W. Jones, Combustion and Flame **7**, p 323 (1963).
31. D.R. Miller, R.L. Evers, and G.B. Skinner, "Effects of Various Inhibitors on Hydrogen-Air Flame Speeds," Combustion and Flame **7**, pp 137-142 (1963).
32. M.J. Day, D.V. Stamp, K. Thompson, and G. Dixon-Lewis, Thirteenth Symposium (International) on Combustion, The Combustion Institute, p 705 (1971).
33. W.E. Wilson, Jr., "Structure, Kinetics, and Mechanism of a Methane-Oxygen Flame Inhibited with Methyl Bromide," Tenth Symposium (International) on Combustion, The Combustion Institute, pp 47-54 (1965).
34. W.E. Wilson, Jr., J.T. O'Donovan, and R.M. Fristrom, "Flame Inhibition by Halogen Compounds," Twelfth Symposium (International) on Combustion, The Combustion Institute, p 929 (1969).

35. G. Dixon-Lewis and R.J. Simpson, "Aspects of Flame Inhibition by Halogen Compounds," Sixteenth Symposium (International) on Combustion, The Combustion Institute, p 1111 (1976).
36. H.Y. Safieh, J. Vandooren, and P.J. Van Tiggelin, "Experimental Study of Inhibition Induced by  $\text{CF}_3\text{Br}$  in a  $\text{CO-H}_2\text{-O}_2\text{-Air}$  Flame," Nineteenth Symposium (International) on Combustion, The Combustion Institute, p.117 (1982).
37. R.F. Simmons and H.G. Wolfhard, "The Influence of Methyl Bromide on Flames," Trans. Faraday Soc. **52**, p 59 (1955).
38. A.M. Dean, J.E. Hardy, and R.K. Lyon, Nineteenth Symposium (International) on Combustion, The Combustion Institute, p 97 (1982).
39. G.J. Minkoff and C.F.H. Tipper, "Chemistry of Combustion Reactions," Butterworths, London, 1962, p 74.
40. B. Lewis and G. von Elbe, "Combustion, Flames and Explosions of Gases," Third Edition, Academic Press, Inc., Orlando, Florida, 1987, p 74.
41. W. Jost, Explosion and Combustion Processes in Gases, First Edition, McGraw-Hill Book Company, Inc., New York and London, 1946, p 304.
42. N. Fujii, H. Miyama, M. Koshi, and T. Asaba, "Kinetics of Ammonia Oxidation in Shock Waves," Eighteenth Symposium (International) on Combustion, The Combustion Institute, pp 873-883 (1981).
43. E.A. Albers, K. Hoyer mann, H.GG. Wagner, and J. Wolfrum, "Study of the Reaction of Ammonia with Oxygen Atoms," Twelfth Symposium (International) on Combustion, The Combustion Institute, P 313 (1969).
44. K. Holzrichter and H.GG. Wagner, "On the Thermal Decomposition of Ammonia Behind Shock Waves," Eighteenth Symposium (International) on Combustion, The Combustion Institute, p 769 (1981).
45. M.E. Morrison and K. Scheller, Combustion and Flame **18**, p 3, (1972).

46. J.W. Hastie, "Molecular Basis of Flame Inhibition," Journal of Research of the National Bureau of Standards-A. Physics and Chemistry **77A**, No. 6, Nov-Dec 1973.
47. C.A. West, J.C.S. **81**, p 923 (1902).
48. G.C. Hampton and A.J. Stosick, J.A.C.S **60**, pp 1814-22 (1938).
49. L. Pauling, The Nature of the Chemical Bond, Cornell University Press, Ithaca, New York, 1960.
50. T.D. Farr, "Phosphorus, Properties of the Element and Some of Its Compounds," Tennessee Valley Authority, Chem. Eng. Rpt. No. 8, p 25 (1950).
51. A.G. Gaydon, Ibid., p 224.
52. G. Herzberg, Infrared and Raman Spectra of Polyatomic Molecules, D. van Nostrand Company, Inc., New York, New York, 1945.
53. A.G. Gaydon, Ibid., pp 313, 324.
54. A.G. Gaydon, Ibid., pp 235, 266.

## TABLES OF OXIDATION MECHANISMS

TABLE I

Hydrogen/Carbon Monoxide Reaction Scheme  
and Rate Coefficients, k.

The units of k for bimolecular reactions are  $\text{cc mol}^{-1} \text{sec}^{-1}$   
and for termolecular reactions,  $\text{cc}^2 \text{mol}^{-2} \text{sec}^{-1}$ .

Reaction	k @ 700K		k @ 1750K	
	Forward	Reverse	Forward	Reverse
1. $\text{OH} + \text{H}_2 \rightleftharpoons \text{H}_2\text{O} + \text{H}$	$5.9 \times 10^{11}$	$4.2 \times 10^7$	$5.6 \times 10^{12}$	$3.1 \times 10^{11}$
2. $\text{H} + \text{O}_2 \rightleftharpoons \text{OH} + \text{O}$	$1.5 \times 10^7$	$1.7 \times 10^{13}$	$3.4 \times 10^{12}$	$2.6 \times 10^{13}$
3. $\text{O} + \text{H}_2 \rightleftharpoons \text{OH} + \text{H}$	$7.3 \times 10^9$	$1.4 \times 10^{10}$	$4.3 \times 10^{12}$	$3.5 \times 10^{12}$
4. $\text{H} + \text{O}_2 + \text{M} \rightleftharpoons \text{HO}_2 + \text{M}^*$	$6.2 \times 10^{15}$	$2.2 \times 10^1$	$4.0 \times 10^{15}$	$7.6 \times 10^9$
5. $\text{CO} + \text{OH} \rightleftharpoons \text{CO}_2 + \text{H}$	$1.3 \times 10^{11}$	$8.4 \times 10^5$	$3.1 \times 10^{11}$	$6.9 \times 10^{10}$
6. $\text{H} + \text{H} + \text{M} \rightleftharpoons \text{H}_2 + \text{M}^*$	$9.5 \times 10^{14}$	$9.7 \times 10^{-18}$	$1.1 \times 10^{15}$	$3.4 \times 10^2$
7. $\text{H} + \text{OH} + \text{M} \rightleftharpoons \text{H}_2\text{O} + \text{M}^*$	$2.4 \times 10^{16}$	$1.8 \times 10^{-20}$	$1.8 \times 10^{16}$	$3.2 \times 10^2$

TABLE II

Methane Oxidation Reaction Scheme and Rate Coefficients,  $k$ The units of  $k$  for bimolecular reactions are  $\text{cc mol}^{-1} \text{sec}^{-1}$   
and for termolecular reactions,  $\text{cc}^2 \text{mol}^{-2} \text{sec}^{-1}$ .

Reaction	$k$ @ 700K		$k$ @ 1750K	
	Forward	Reverse	Forward	Reverse
8. $\text{CH}_4 + \text{M} \rightleftharpoons \text{CH}_3 + \text{H} + \text{M}^*$	$2.0 \times 10^{-11}$	$1.3 \times 10^{20}$	$8.3 \times 10^5$	$11 \times 10^{17}$
9. $\text{CH}_4 + \text{O}_2 \rightleftharpoons \text{CH}_3 + \text{HO}_2$	$6.0 \times 10^{-1}$	N/A	$2.0 \times 10^8$	N/A
10. $\text{O}_2 + \text{M} \rightleftharpoons \text{O} + \text{O} + \text{M}^*$	$8.7 \times 10^{-20}$	N/A	2.7	N/A
11. $\text{CH}_4 + \text{O} \rightleftharpoons \text{CH}_3 + \text{OH}$	$4.1 \times 10^{10}$	$5.3 \times 10^9$	$6.5 \times 10^{12}$	$2.1 \times 10^{11}$
12. $\text{CH}_4 + \text{H} \rightleftharpoons \text{CH}_3 + \text{H}_2$	$2.6 \times 10^{10}$	$1.7 \times 10^9$	$4.9 \times 10^{12}$	$1.9 \times 10^{11}$
13. $\text{CH}_4 + \text{OH} \rightleftharpoons \text{CH}_3 + \text{H}_2\text{O}$	$8.1 \times 10^{11}$	$3.9 \times 10^6$	$7.1 \times 10^{12}$	$1.6 \times 10^{10}$
14. $\text{CH}_3 + \text{O} \rightleftharpoons \text{HCHO} + \text{H}$	$6.1 \times 10^{13}$	$3.8 \times 10^{-7}$	$1.5 \times 10^{14}$	$6.3 \times 10^6$
15. $\text{CH}_3 + \text{O}_2 \rightleftharpoons \text{HCHO} + \text{OH}$	$10^{11}$ to $10^{14}$	est.	$10^{11}$ to $10^{14}$	est.
16. $\text{HCHO} + \text{OH} \rightleftharpoons \text{HCO} + \text{H}_2\text{O}$	$2.2 \times 10^{13}$	$4.2 \times 10^2$	$5.6 \times 10^{13}$	$1.3 \times 10^9$
17. $\text{HCO} + \text{OH} \rightleftharpoons \text{CO} + \text{H}_2\text{O}$	$10^{12}$ to $10^{15}$	est.	$10^{12}$ to $10^{15}$	est.
18. $\text{CO} + \text{OH} \rightleftharpoons \text{CO}_2 + \text{H}$	$1.3 \times 10^{11}$	$8.4 \times 10^5$	$3.1 \times 10^{11}$	$6.9 \times 10^{10}$
19. $\text{H} + \text{O}_2 \rightleftharpoons \text{OH} + \text{O}$	$1.5 \times 10^9$	$1.7 \times 10^{13}$	$3.4 \times 10^{12}$	$2.6 \times 10^{13}$
20. $\text{O} + \text{H}_2 \rightleftharpoons \text{OH} + \text{H}$	$7.3 \times 10^9$	$1.4 \times 10^{10}$	$4.3 \times 10^{12}$	$3.5 \times 10^{12}$
21. $\text{O} + \text{H}_2\text{O} \rightleftharpoons \text{OH} + \text{OH}$	$1.1 \times 10^8$	$2.9 \times 10^{12}$	$3.2 \times 10^{11}$	$4.5 \times 10^{12}$
22. $\text{H} + \text{H}_2\text{O} \rightleftharpoons \text{H}_2 + \text{OH}$	$4.2 \times 10^7$	$5.9 \times 10^{11}$	$3.1 \times 10^{11}$	$5.6 \times 10^{12}$
23. $\text{H} + \text{OH} + \text{M} \rightleftharpoons \text{H}_2\text{O} + \text{M}^*$	$2.4 \times 10^{16}$	$1.8 \times 10^{-20}$	$1.8 \times 10^{16}$	$3.2 \times 10^2$
24. $\text{CH}_3 + \text{O}_2 \rightleftharpoons \text{HCO} + \text{H}_2\text{O}$	$10^{11}$ to $10^{12}$	est.	$10^{11}$ to $10^{12}$	est.
25. $\text{HCO} + \text{M} \rightleftharpoons \text{H} + \text{CO} + \text{M}^*$	$5.0 \times 10^5$	N/A	$2.1 \times 10^{11}$	N/A

TABLE III

N/H/O Reaction Scheme and Rate Coefficients

The units of k are  $\text{cc m}^{-1} \text{sec}^{-1}$ 

Reaction	k @ 700K		k @ 1750K	
	Forward	Reverse	Forward	Reverse
26. $\text{NH}_3 + \text{M}^* \rightarrow \text{NH}_2 + \text{H} + \text{M}$	$1.3 \times 10^{-13}$	N/A	$4.9 \times 10^4$	N/A
27. $\text{NH}_3 + \text{H} \rightarrow \text{NH}_2 + \text{H}_2$	$1.3 \times 10^{12}$	$6.4 \times 10^{10}$	$1.0 \times 10^{13}$	$8.0 \times 10^{11}$
28. $\text{NH}_3 + \text{O} \rightarrow \text{NH}_2 + \text{OH}$	$2.0 \times 10^{10}$	$1.9 \times 10^9$	$2.7 \times 10^{11}$	$1.7 \times 10^{10}$
29. $\text{NH}_3 + \text{OH} \rightarrow \text{NH}_2 + \text{H}_2\text{O}$	$1.2 \times 10^{12}$	$4.2 \times 10^6$	$3.5 \times 10^{12}$	$1.5 \times 10^{10}$
30. $\text{NH}_2 + \text{H} \rightarrow \text{NH} + \text{H}_2$	$5.1 \times 10^{11}$	$7.1 \times 10^{10}$	$6.0 \times 10^{12}$	$2.0 \times 10^{12}$
31. $\text{NH}_2 + \text{O} \rightarrow \text{NH} + \text{OH}$	$2.4 \times 10^{13}$	$6.6 \times 10^{12}$	$3.9 \times 10^{13}$	$1.1 \times 10^{13}$
32. $\text{NH}_2 + \text{O} \rightarrow \text{HNO} + \text{H}$	$2.4 \times 10^{13}$	N/A	$1.5 \times 10^{13}$	N/A
33. $\text{NH}_2 + \text{OH} \rightarrow \text{NH} + \text{H}_2\text{O}$	$1.0 \times 10^{12}$	$1.0 \times 10^7$	$3.3 \times 10^{12}$	$6.4 \times 10^{10}$
34. $\text{N} + \text{H}_2 \rightarrow \text{NH} + \text{H}$	$2.6 \times 10^{12}$	$5.2 \times 10^{10}$	$3.1 \times 10^{13}$	$2.6 \times 10^{12}$
35. $\text{NH} + \text{O} \rightarrow \text{NO} + \text{H}$	$1.7 \times 10^{13}$	$2.0 \times 10^{-10}$	$2.6 \times 10^{13}$	$5.5 \times 10^4$
36. $\text{NH} + \text{O} \rightarrow \text{N} + \text{OH}$	$5.5 \times 10^{10}$	N/A	$1.7 \times 10^{12}$	N/A
37. $\text{NH} + \text{OH} \rightarrow \text{HNO} + \text{H}$	$6.3 \times 10^{12}$	N/A	$1.5 \times 10^{13}$	N/A
38. $\text{NH} + \text{OH} \rightarrow \text{N} + \text{H}_2\text{O}$	$3.1 \times 10^{12}$	$7.5 \times 10^{-1}$	$1.2 \times 10^{13}$	$6.7 \times 10^8$
39. $\text{HNO} + \text{H} \rightarrow \text{NO} + \text{H}_2$	$7.2 \times 10^{11}$	N/A	$4.0 \times 10^{12}$	N/A
40. $\text{HNO} + \text{OH} \rightarrow \text{H}_2\text{O} + \text{NO}$	$4.9 \times 10^{11}$	$9.8 \times 10^{-11}$	$7.5 \times 10^{11}$	$2.8 \times 10^3$
41. $\text{HNO} + \text{O} \rightarrow \text{OH} + \text{NO}$	$1.3 \times 10^{13}$	$7.2 \times 10^{-5}$	$2.1 \times 10^{13}$	$1.1 \times 10^6$

TABLE IV

N/H/O Reactions Involving HO<sub>2</sub>  
and Rate Coefficients, k, at 700K

The units of k are cc mol<sup>-1</sup> sec<sup>-1</sup>

Reaction		k @ 700K	
		Forward	Reverse
42.	NH <sub>3</sub> + HO <sub>2</sub> ⇌ NH <sub>2</sub> + H <sub>2</sub> O <sub>2</sub>	9.0×10 <sup>4</sup>	N/A
43.	NH <sub>2</sub> + HO <sub>2</sub> ⇌ NH <sub>3</sub> + O <sub>2</sub>	2.4×10 <sup>12</sup>	N/A
44.	NH <sub>2</sub> + HO <sub>2</sub> ⇌ NH + H <sub>2</sub> O <sub>2</sub>	2.4×10 <sup>12</sup>	N/A
45.	NH + HO <sub>2</sub> ⇌ HNO + OH	2.4×10 <sup>12</sup>	N/A
46.	N + HO <sub>2</sub> ⇌ NO + OH	2.4×10 <sup>12</sup>	N/A
47.	N + HO <sub>2</sub> ⇌ NH + O <sub>2</sub>	2.4×10 <sup>12</sup>	N/A
48.	NO + HO <sub>2</sub> ⇌ HNO + O <sub>2</sub>	4.8×10 <sup>10</sup>	N/A
49.	NO + HO <sub>2</sub> ⇌ NO <sub>2</sub> + OH	1.0×10 <sup>12</sup>	7.1×10 <sup>9</sup>
50.	HNO + HO <sub>2</sub> ⇌ NO + H <sub>2</sub> O <sub>2</sub>	7.6×10 <sup>10</sup>	N/A

## TABLES OF EXPERIMENTAL RESULTS

TABLE V

IR Spectral Emission of Opposed-Jet Diffusion Flame  
 Methane (undiluted)/Air, Overall  $\phi = 0.86$   
 1.6% Methyl Bromide Added to Air Side

3700-2700  $\text{cm}^{-1}$

	Slit Position (in.)	Spectral Area ( $\text{in}^2$ )		% Change
		Without MeBr	With MeBr	
Fuel Side	0.00	4.27	0.06	-98.6
		7.04	7.03	- 0.1
		9.83	10.46	6.4
		11.95	13.87	16.1
	0.05	16.21	17.73	9.4
		19.66	21.85	11.1
		21.00	25.73	22.5
		16.94	22.93	35.4
	0.10	12.82	16.64	29.8
		8.95	11.51	28.6
		7.77	8.98	15.6
		7.64	8.46	10.7
	0.15	6.97	8.53	22.4
		7.22	8.51	17.9
7.46		8.25	10.5	
6.87		7.67	11.6	
0.20	6.07	6.96	14.7	
	5.10	6.12	20.0	
	4.24	4.86	14.6	
	3.03	3.44	12.5	
Oxygen Side	0.24	2.16	6.68	24.1
		1.10	1.77	60.9
		0.73	1.31	79.5
		0.53	0.79	49.1
		N/A	0.00	-
	TOTAL	195.56	226.14	15.64

TABLE VI

IR Spectral Emission of Opposed-Jet Diffusion Flame  
 Methane (undiluted)/Air, Overall  $\phi = 0.86$   
 1.6% Methyl Bromide Added to Air Side

2450-2000  $\text{cm}^{-1}$

	Slit Position (in.)	Spectral Area ( $\text{in}^2$ )		
		Without MeBr	With MeBr	% Change
Fuel Side	0.00	0.32	0.18	-43.7
		0.48	0.55	14.6
		0.84	0.30	- 4.8
	0.05	1.00	1.06	6.0
		1.41	1.35	- 4.4
		1.70	1.76	3.5
		2.60	2.14	-17.7
		2.65	2.30	-13.2
		2.89	2.51	-13.2
	0.10	3.23	3.37	4.3
		3.83	3.74	- 2.4
		4.29	4.40	2.6
		4.80	5.01	4.4
		5.25	5.41	3.1
	0.15	5.47	5.75	5.1
		5.55	5.75	3.6
5.25		5.28	0.6	
4.53		4.97	9.7	
0.20	3.87	4.25	9.8	
	3.02	3.32	10.6	
	2.15	2.60	20.9	
Oxygen Side	1.53	1.86	21.6	
	1.01	1.85	23.8	
	0.55	0.74	34.6	
0.24	0.25	0.07	-72.0	
TOTAL		68.47	70.44	2.9

TABLE VII

IR Spectral Emission of Opposed-Jet Diffusion Flame  
 Methane (undiluted)/Air, Overall  $\phi = 0.86$   
 1.6% Methyl Bromide Added to Air Side

Peak at  $3470 \text{ cm}^{-1}$

	Slit Position (in.)	Spectral Area ( $\text{in}^2$ )			
		Without MeBr	With MeBr	% Change	
Fuel Side	0.08	3.86	N/A	-	
		3.06	3.48	13.7	
	0.10	3.17	3.14	- 0.5	
		3.63	3.80	4.7	
		4.28	4.50	5.1	
		4.86	5.34	9.9	
		5.43	5.89	8.5	
		0.15	5.68	5.73	0.1
			5.17	5.55	7.4
			4.36	4.93	13.1
	3.49	3.80	8.9		
Oxygen Side	0.20	2.69	3.00	11.5	
		1.76	2.00	13.6	
	TOTAL	47.58	51.16	7.5	

TABLE VIII

IR Spectral Emission of Opposed-Jet Diffusion Flame  
Methane (undiluted)/Air, Overall  $\phi = 0.86$   
1.6% Methyl Bromide Added to Air Side

Peak at  $3000\text{ cm}^{-1}$

	Slit Position (in.)	Spectral Area ( $\text{in}^2$ )		
		Without MeBr	With MeBr	% Change
Fuel Side	0.08	6.00	7.33	22.0
		3.60	4.87	35.3
	0.10	2.61	3.33	27.6
		2.22	2.58	16.2
		1.79	2.21	23.5
Oxygen Side	0.15	1.21	1.72	42.2
		0.81	1.19	46.9
	0.15	0.51	0.84	64.7
		0.00	0.48	-
		0.00	0.41	-
TOTAL	18.75	24.96	33.1	

TABLE IX

Effect of MeBr on Extreme Flame Edge Emission of  $\text{CO}_2/\text{CO}$   
Methane/Oxygen/Nitrogen,  $\phi = 2.0$   
0.6% Methyl Bromide Added to Fuel Side  
Average Spectral Areas ( $\text{in}^2$ )

$2400\text{ to }2000\text{ cm}^{-1}$

	Without MeBr	With MeBr	% Change
Fuel Side:	0.541	0.473	- 12.6
Oxygen Side:	0.418	0.361	- 13.6

TABLE X

IR Spectral Emission of Opposed-Jet Diffusion Flame  
 Hydrogen-Carbon Monoxide-Nitrogen/Oxygen-Nitrogen  
 Overall  $\phi = 0.86$

3.0% Methyl Bromide Added to Oxygen Side

3800-2900  $\text{cm}^{-1}$

	Slit Position (in.)	Spectral Area ( $\text{in}^2$ )		
		Without MeBr	With MeBr	% Change
Fuel Side	0.18	0.24	0.09	-62.5
		0.17	0.28	64.7
		0.35	0.31	-11.4
	0.23	0.58	0.72	24.1
		1.19	1.37	15.1
		1.70	2.04	20.0
		2.70	3.00	11.1
		3.77	4.37	15.9
		5.13	5.95	16.0
		6.75	7.32	8.4
	0.28	8.00	9.19	14.9
		9.36	10.97	17.2
		10.91	11.45	4.9
		10.87	12.48	14.8
	0.33	11.42	12.47	9.2
11.39		11.54	1.3	
10.30		10.52	2.1	
9.07		8.82	- 2.8	
6.84		6.77	- 1.0	
0.38	5.23	4.86	- 7.1	
	2.41	2.52	4.6	
	0.85	0.74	-12.9	
Air Side	0.40	0.00	-100.0	
	TOTAL	119.29	127.78	7.1

TABLE XI

IR Spectral Emission of Opposed-Jet Diffusion Flame  
 Hydrogen-Carbon Monoxide-Nitrogen/Oxygen-Nitrogen  
 Overall  $\phi = 0.86$

3.0% Methyl Bromide Added to Oxygen Side

2400-2000  $\text{cm}^{-1}$

	Slit Position (in.)	Spectral Area ( $\text{in}^2$ )		
		Without MeBr	With MeBr	% Change
Fuel Side	0.17	0.65	0.67	3.1
		0.89	0.93	4.5
		1.30	1.27	- 2.3
		1.61	1.71	6.2
		1.97	2.14	8.6
	0.23	2.45	2.63	7.3
		2.96	3.24	9.5
		3.48	3.78	8.6
		4.32	4.46	3.2
		4.93	5.09	3.2
	0.28	5.15	5.54	7.6
		5.69	6.24	9.7
		6.20	6.40	3.2
		6.24	6.49	4.0
		6.15	6.66	8.3
0.33	6.20	6.25	0.8	
	6.10	6.14	0.7	
	5.44	5.42	- 0.2	
	4.82	5.07	5.2	
	4.05	4.19	3.5	
0.38	3.02	3.02	0.0	
	1.80	1.96	8.9	
	0.77	0.85	10.4	
Air Side	0.40	0.09	-44.4	
	TOTAL	87.08	90.20	3.6

TABLE XII

IR Spectral Emission of Opposed-Jet Diffusion Flame  
 Hydrogen-Carbon Monoxide-Nitrogen/Oxygen-Nitrogen  
 Overall  $\phi = 0.86$

0.6% Methyl Bromide Added to Fuel Side

3800-2900  $\text{cm}^{-1}$

	Slit Position (in.)	Spectral Area ( $\text{in}^2$ )		
		Without MeBr	With MeBr	% Change
Fuel Side	0.18	0.00	0.00	0.0
		0.03	0.10	233.3
		0.14	0.15	7.1
		0.31	0.20	-35.5
		0.57	0.68	19.3
	0.23	1.47	1.38	- 6.1
		2.45	2.26	- 7.8
		3.27	3.12	- 4.6
		4.59	4.45	- 3.1
		5.60	5.92	5.7
	0.28	7.27	7.37	1.4
		8.42	8.58	1.9
		9.39	9.40	0.1
		9.65	9.70	0.5
		9.54	9.49	- 0.5
0.33	8.64	8.78	1.6	
	7.61	7.65	0.5	
	6.19	6.14	- 0.8	
	4.63	4.45	- 3.9	
	2.81	2.66	- 5.3	
0.38	1.25	1.06	- 5.2	
	0.07	0.08	-12.5	
Air Side	0.40	0.00	0.0	
	TOTAL	93.90	93.62	- 0.3

TABLE XIII

IR Spectral Emission of Opposed-Jet Diffusion Flame  
 Hydrogen-Carbon Monoxide-Nitrogen/Oxygen-Nitrogen  
 Overall  $\phi = 0.86$

0.6% Methyl Bromide Added to Fuel Side

2450-2000  $\text{cm}^{-1}$

	Slit Position (in.)	Spectral Area ( $\text{in}^2$ )		
		Without MeBr	With MeBr	% Change
Fuel Side	0.17	0.50	0.55	0.0
		0.65	0.74	13.8
	0.23	1.01	0.89	-11.9
		1.23	1.21	- 1.6
		1.55	1.66	7.1
		1.87	1.93	3.2
		2.49	2.54	2.0
		2.88	3.08	6.9
	0.28	3.50	3.63	3.7
		3.89	4.06	4.4
		4.43	4.60	3.8
		4.80	5.00	4.2
		5.12	5.15	0.6
		5.35	5.38	0.6
0.33	5.25	5.37	2.9	
	4.98	5.33	7.0	
	4.67	4.78	2.4	
	4.06	4.34	6.9	
	3.47	3.46	- 0.3	
	2.70	2.94	8.9	
0.38	1.79	1.91	6.7	
	1.12	1.10	- 1.8	
Oxygen Side	0.38	0.40	5.3	
	0.40	0.00	0.0	
TOTAL		67.69	70.05	3.5

TABLE XIV

IR Spectral Emission of Opposed-Jet Diffusion Flame  
 Hydrogen-Carbon Monoxide-Nitrogen/Oxygen-Nitrogen  
 Overall  $\phi = 0.5$   
 0.2% Methyl Bromide Added to Fuel Side

3800-2700  $\text{cm}^{-1}$

	Slit Position (in.)	Spectral Area ( $\text{in}^2$ )		
		Without MeBr	With MeBr	% Change
Fuel	0.105	0.87	0.72	-17.2
Side	0.140	5.06	5.87	16.0
	0.175	9.09	9.96	9.6
	0.210	8.86	8.86	0.0
	0.245	4.58	4.88	6.6
Oxygen	0.280	1.21	1.20	- 0.8
Side	0.315	0.16	0.21	31.3
	TOTAL	29.83	31.70	6.3

2450-2000  $\text{cm}^{-1}$

	Slit Position (in.)	Spectral Area ( $\text{in}^2$ )		
		Without MeBr	With MeBr	% Change
Fuel	0.105	1.25	1.29	- 4.8
Side	0.140	3.93	4.39	11.7
	0.175	5.59	6.10	9.1
	0.210	4.80	5.41	12.7
	0.245	3.38	3.25	- 3.8
Oxygen	0.280	1.36	1.47	8.1
Side	0.315	0.43	0.47	9.3
	TOTAL	20.74	22.28	7.4

TABLE XV

IR Spectral Emission of Opposed-Jet Diffusion Flame  
 Hydrogen-Carbon Monoxide-Nitrogen/Oxygen-Nitrogen  
 Overall  $\phi=0.5$   
 Comparison of MeBr Addition to Fuel Side and Oxygen Side  
 0.2% Methyl Bromide Added to Indicated Side

2450-2000  $\text{cm}^{-1}$ 

Slit Position (in.)		Spectral Area ( $\text{in}^2$ )				
		w/o MeBr	With MeBr		% Change	
			Fuel	Oxy	Fuel	Oxy
Fuel	0.100	0.61	0.74	0.66	21.3	8.2
Side	0.130	3.71	3.72	3.81	0.3	2.7
	0.160	5.19	5.20	5.30	0.3	2.1
	0.190	4.97	5.32	5.39	7.0	8.5
	0.220	3.93	4.00	4.22	1.8	7.4
Oxy	0.250	2.09	2.18	2.32	4.3	11.0
Side	0.280	0.73	0.78	0.96	6.8	31.5
TOTAL		21.23	21.94	22.66	3.3	6.7

TABLE XVI

IR Spectral Emission of Opposed-Jet Diffusion Flame  
 Hydrogen-Carbon Monoxide-Nitrogen/Oxygen-Nitrogen  
 Overall  $\phi=0.5$   
 0.2% Methyl Bromide Added to Oxygen Side

2450-2000  $\text{cm}^{-1}$ 

Slit Position (in.)		Spectral Area ( $\text{in}^2$ )		
		w/o MeBr	With MeBr	% Change
Fuel	0.120	1.00	1.11	11.0
Side	0.150	2.66	2.77	4.1
	0.180	4.29	4.37	1.9
	0.210	5.07	4.84	- 4.5
	0.240	3.73	3.90	4.6
Oxy	0.270	1.90	1.84	- 3.2
Side	0.300	0.46	0.53	15.2
TOTAL		19.11	19.36	1.3

TABLE XVII

IR Spectral Emission of Opposed-Jet Diffusion Flame  
 Methane-Nitrogen/Oxygen-Nitrogen, Overall  $\phi=2.0$   
 0.21% Ammonia Added to Oxygen Side  
 Repeated Scans at Fixed Position

2450 - 2000  $\text{cm}^{-1}$

Slit Position (in.)	Spectral Area ( $\text{in}^2$ )			
	Without $\text{NH}_3$	With $\text{NH}_3$	% Change	
Fuel Side 0.225	1.135	1.210		
	1.125	1.250		
	1.270	1.295		
	Average:	1.177	1.252	6.4
	Range:	0.145	0.085	
Oxy Side 0.375	1.300	1.300		
	1.265	1.300		
	1.240	1.385		
	Average:	1.268	1.328	4.7
	Range:	0.060	0.085	

TABLE XVIII

IR Spectral Emission of Opposed-Jet Diffusion Flame  
 Methane-Nitrogen/Oxygen-Nitrogen, Overall  $\phi=0.5$   
 0.21% Ammonia Added to Oxygen Side  
 Repeated Scans at Fixed Position

2450 - 2000  $\text{cm}^{-1}$

Slit Position (in.)	Spectral Area ( $\text{in}^2$ )		
	Without $\text{NH}_3$	With $\text{NH}_3$	% Change
Fuel Side 0.225	1.105	1.260	
	1.150	1.200	
Average:	1.128	1.230	9.0
Range:	0.045	0.060	
Oxy Side 0.370	1.400	1.515	
	1.585	1.540	
Average:	1.493	1.528	2.3
Range:	0.085	0.025	

TABLE XIX

IR Spectral Emission of Opposed-Jet Diffusion Flame  
Methane-Nitrogen/Oxygen-Nitrogen, Overall  $\phi=1.0$   
0.21% Ammonia Added to Oxygen Side

2450 - 2000  $\text{cm}^{-1}$

Slit Position (in.)	Spectral Area ( $\text{in}^2$ )		
	Without $\text{NH}_3$	With $\text{NH}_3$	% Change
Fuel Side 0.215	0.285	0.340	19.3
0.245	1.225	1.370	11.8
0.275	3.070	3.110	1.3
Mid-flame 0.305	4.900	4.910	0.0

Peak at 3000  $\text{cm}^{-1}$  (3020-2800  $\text{cm}^{-1}$ )

Slit Position (in.)	Spectral Area ( $\text{in}^2$ )		
	Without $\text{NH}_3$	With $\text{NH}_3$	% Change
Fuel Side 0.215	0.195	0.225	15.4
0.245	1.210	1.355	12.0
0.275	1.545	1.700	10.0
Mid-flame 0.305	0.255	0.320	25.5

3800 - 3020  $\text{cm}^{-1}$

Slit Position (in.)	Spectral Area ( $\text{in}^2$ )		
	Without $\text{NH}_3$	With $\text{NH}_3$	% Change
Fuel Side 0.215	Bigger	Smaller	N/A
0.245	0.51 (1.03)*	0.42 (1.02)*	- 6.5
0.275	5.700	5.650	- 0.9
Mid-flame 0.305	9.630	9.970	3.5

\* Note: Between 3800 and 3020  $\text{cm}^{-1}$  there are two bands that are easily separated at this position in the flame. The numbers in parentheses are for the band 3300 to 3020  $\text{cm}^{-1}$  and the others are for the band 3800 to 3300  $\text{cm}^{-1}$ .

TABLE XX

IR Spectral Emission of Opposed-Jet Diffusion Flame  
 Methane-Nitrogen/Oxygen-Nitrogen, Overall  $\phi=1.0$   
 0.21% Ammonia Added to Oxygen Side  
 Repeated Scans at Fixed Position

2350 - 2200  $\text{cm}^{-1}$

Slit Position (in.)	Average Spectral Area ( $\text{in}^2$ )		
	Without $\text{NH}_3$	With $\text{NH}_3$	% Change
Extreme Fuel Side	0.479	0.420	-12.3
Extreme Oxygen Side	0.378	0.424	12.2

TABLE XXI

IR Spectral Emission of Opposed-Jet Diffusion Flame  
 Methane-Nitrogen/Oxygen-Nitrogen, Overall  $\phi=1.0$   
 0.21% Ammonia Added to Oxygen Side  
 Repeated Scans at Fixed Position

2350 - 2200  $\text{cm}^{-1}$

Slit Position (in.)	Average Spectral Area ( $\text{in}^2$ )		
	Without $\text{NH}_3$	With $\text{NH}_3$	% Change
Extreme Fuel Side	0.483	0.428	-11.4

3600 - 3000  $\text{cm}^{-1}$

Slit Position (in.)	Average Spectral Area ( $\text{in}^2$ )		
	Without $\text{NH}_3$	With $\text{NH}_3$	% Change
Extreme Oxygen Side	0.143	0.208	45.5

TABLE XXII

IR Spectral Emission of Opposed-Jet Diffusion Flame  
 Hydrogen-Carbon Monoxide-Nitrogen/Oxygen-Nitrogen  
 Overall  $\phi=1.0$

0.21% Ammonia Added to Oxygen Side

Repeated Scans at Fixed Position

2400 - 2100  $\text{cm}^{-1}$

Slit Position (in.)	Spectral Area ( $\text{in}^2$ )		
	Without $\text{NH}_3$	With $\text{NH}_3$	% Change
Oxygen Side	1.300	1.390	
	1.260	1.460	
Average:	1.280	1.425	11.3
Range:	0.040	0.070	

3800 - 3100  $\text{cm}^{-1}$

Slit Position (in.)	Spectral Area ( $\text{in}^2$ )		
	Without $\text{NH}_3$	With $\text{NH}_3$	% Change
Oxygen Side	1.990	2.150	
	1.940	2.120	
Average:	1.965	2.135	8.7
Range:	0.050	0.030	

TABLE XXIII

IR Spectral Emission of Opposed-Jet Diffusion Flame  
 Hydrogen-Carbon Monoxide-Nitrogen/Oxygen-Nitrogen  
 Overall  $\phi=1.0$   
 0.21% Ammonia Added to Oxygen Side  
 Repeated Scans at Fixed Position

2400 - 2100  $\text{cm}^{-1}$

Slit Position (in.)	Spectral Area ( $\text{in}^2$ )		
	Without $\text{NH}_3$	With $\text{NH}_3$	% Change
Extreme Oxygen Side	0.420	0.520	
	0.405	0.505	
	0.445	0.470	
Average:	0.423	0.498	17.7
Range:	0.040	0.050	

TABLE XXIV

IR Spectral Emission of Opposed-Jet Diffusion Flame  
 Hydrogen-Carbon Monoxide-Nitrogen/Oxygen-Nitrogen  
 Overall  $\phi = 2.0$   
 100 ppm  $P_4O_{10}$  Added to Oxygen Side

3800-2700  $cm^{-1}$

	Slit Position (in.)	Spectral Area ( $in^2$ )		
		Without $P_4O_{10}$	With $P_4O_{10}$	% Change
Fuel	0.130	1.23	2.85	131.7
Side	0.170	2.14	2.47	15.4
	0.210	6.52	6.87	5.4
	0.250	12.04	13.30	10.5
	0.290	13.22	14.76	11.6
Oxygen Side	0.330	8.03	9.47	17.9
	0.370	0.76	1.03	35.5
	TOTAL	43.94	50.75	15.5

2450-2000  $cm^{-1}$

	Slit Position (in.)	Spectral Area ( $in^2$ )		
		Without $P_4O_{10}$	With $P_4O_{10}$	% Change
Fuel	0.130	1.26	1.42	12.7
Side	0.170	2.43	2.70	11.1
	0.210	4.10	4.46	8.8
	0.250	5.37	5.85	8.9
	0.290	5.12	5.49	7.2
Oxygen Side	0.330	3.31	3.88	17.2
	0.370	0.74	0.72	- 2.7
	TOTAL	22.33	24.52	9.8

TABLE XXV

IR Spectral Emission of Opposed-Jet Diffusion Flame  
Hydrogen-Carbon Monoxide-Nitrogen/Oxygen-Nitrogen

Overall  $\phi = 0.5$

100 ppm  $P_4O_{10}$  Added to Oxygen Side

3800-2700  $cm^{-1}$

	Slit Position (in.)	Spectral Area ( $in^2$ )		
		Without $P_4O_{10}$	With $P_4O_{10}$	% Change
Fuel	0.110	0.00	0.05	-
Side	0.145	1.62	2.34	44.4
	0.180	6.90	8.09	17.2
	0.215	9.60	10.89	13.4
	0.250	6.03	7.07	17.2
Oxygen	0.285	1.11	1.81	63.1
Side	0.310	0.00	0.14	-
	TOTAL	25.26	30.39	20.3

2450-2000  $cm^{-1}$

	Slit Position (in.)	Spectral Area ( $in^2$ )		
		Without $P_4O_{10}$	With $P_4O_{10}$	% Change
Fuel	0.110	0.74	0.90	21.6
Side	0.145	2.62	3.00	14.5
	0.180	4.69	5.19	10.7
	0.215	5.47	5.84	6.8
	0.250	4.04	4.35	7.7
Oxygen	0.285	1.60	1.88	17.5
Side	0.310	0.45	0.66	46.7
	TOTAL	19.61	21.82	11.3

TABLE XXVI

IR Spectral Emission of Opposed-Jet Diffusion Flame  
 Methane-Nitrogen/Oxygen-Nitrogen, Overall  $\phi = 1.0$   
 100 ppm  $P_4O_{10}$  Added to Oxygen Side  
 Repeated Scans at Extreme Flame Edges

2450-2000  $cm^{-1}$

Slit Position (in.)	Spectral Area ( $in^2$ )		
	Without $P_4O_{10}$	With $P_4O_{10}$	% Change
Fuel Side 0.198	0.284	0.319	12.3
Oxy Side 0.383	0.358	0.380	6.2

3100-2900  $cm^{-1}$

Slit Position (in.)	Spectral Area ( $in^2$ )		
	Without $P_4O_{10}$	With $P_4O_{10}$	% Change
Fuel Side 0.194	0.301	0.369	22.6
Oxy Side - No Emission Between 4000 and 2450 $cm^{-1}$ on Oxygen-Side Edge.			

## FIGURES

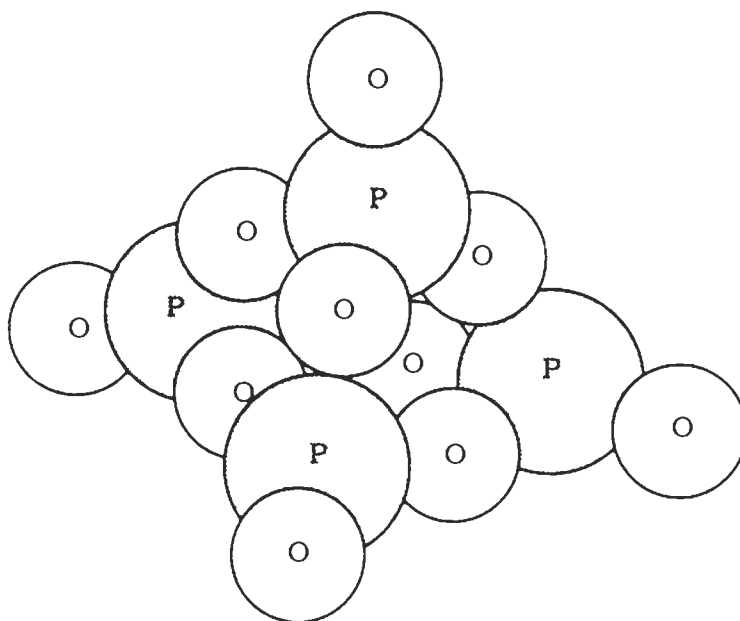


Fig. 1.  $P_4O_{10}$  molecule

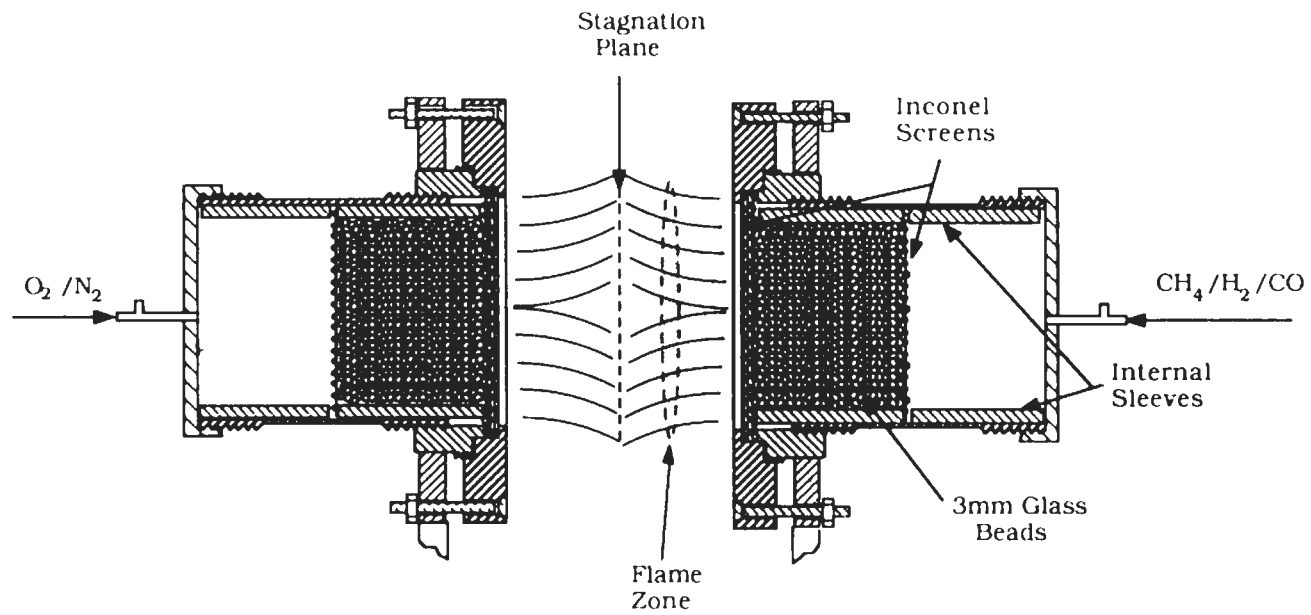


Figure 2. Burner Tube Assembly

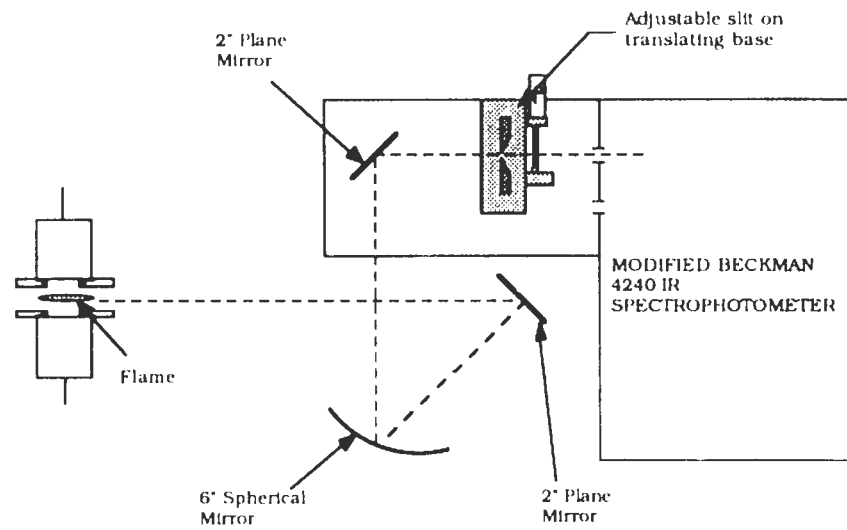


Figure 3. Optical System

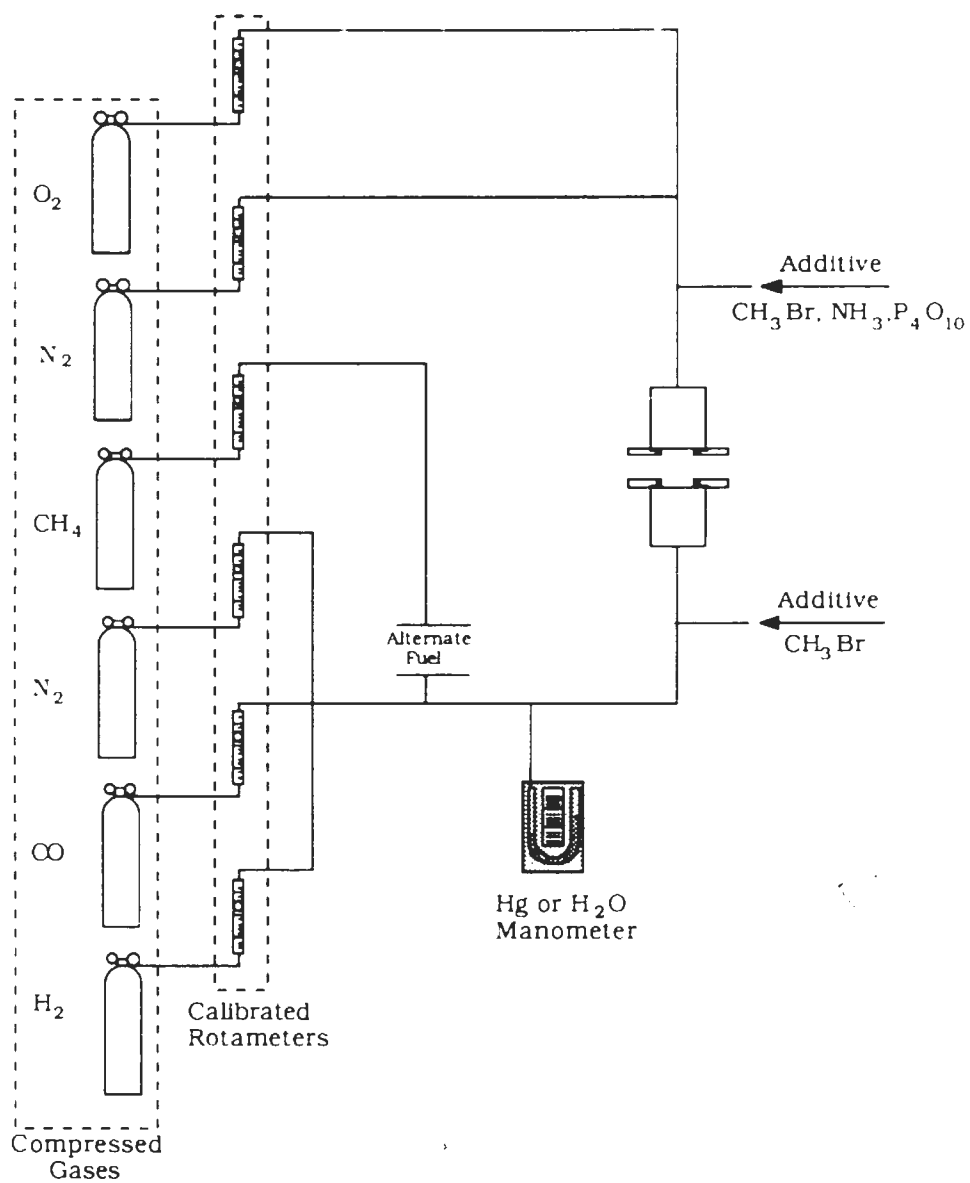


Figure 4. Gas Control System

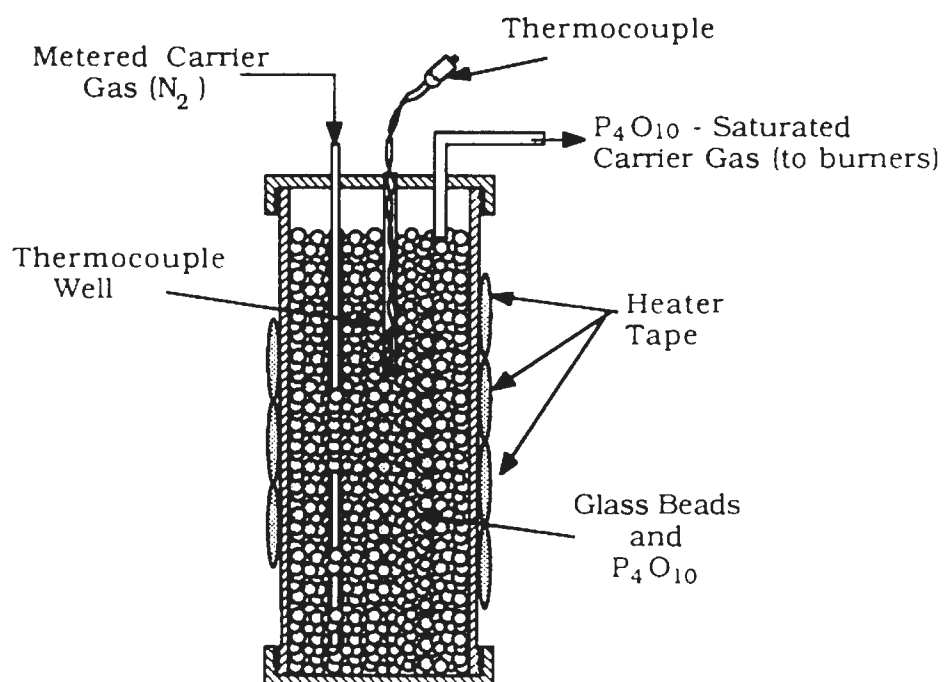


Figure 5.  $P_4O_{10}$  Addition System

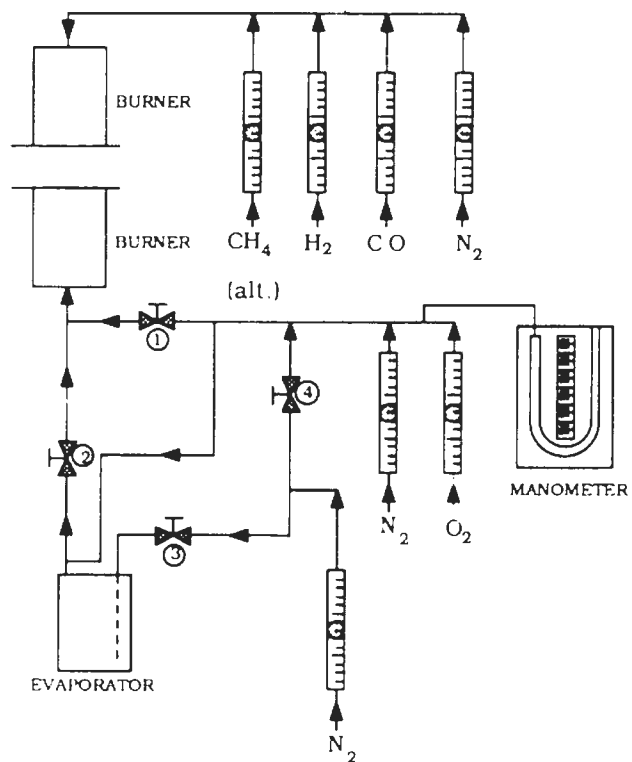


Figure 6.  $P_4O_{10}$  Pressure Equilization System

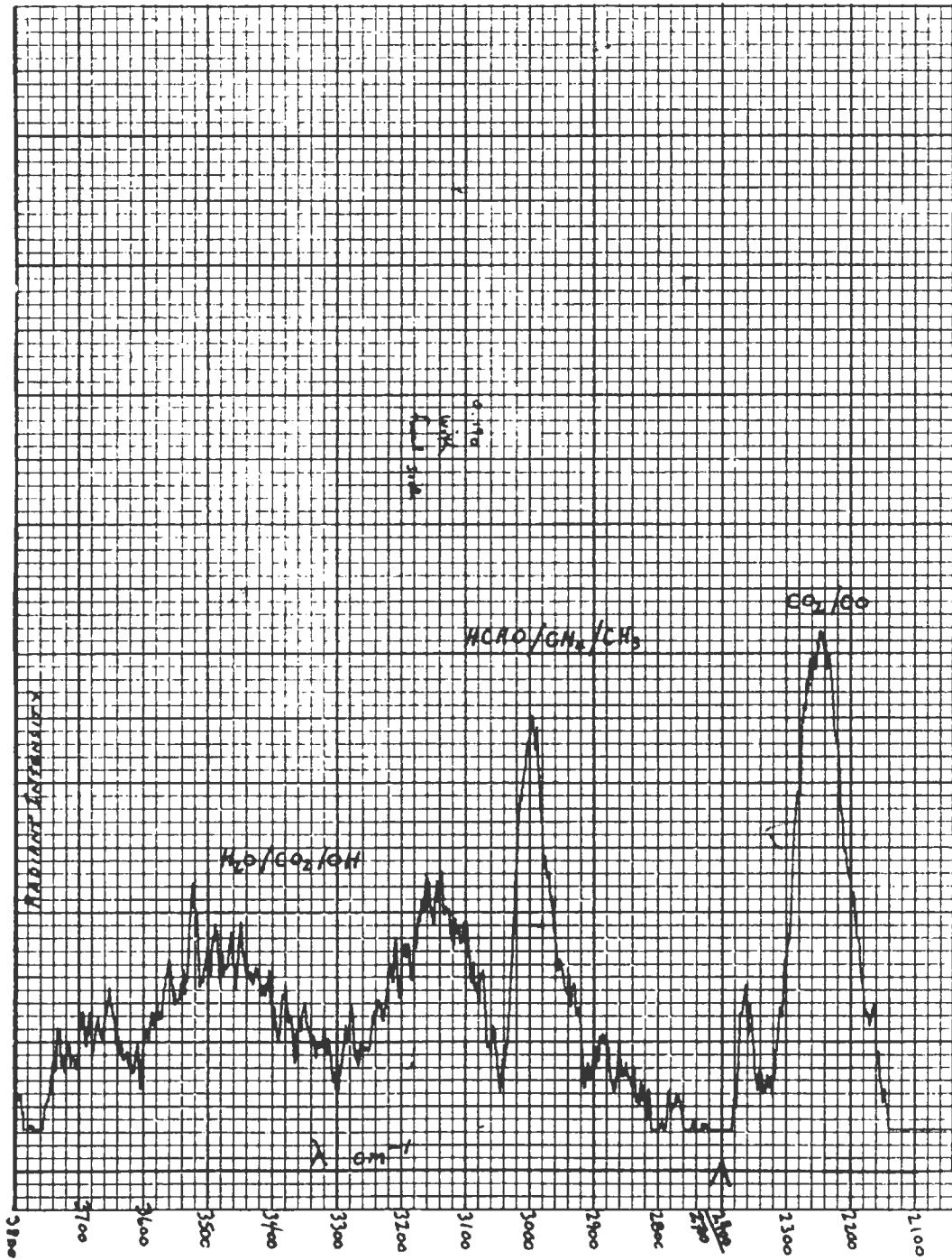


Figure 7a. Infrared Emission of Methane/Air Opposed-Jet Diffusion Flame - Fuel Side

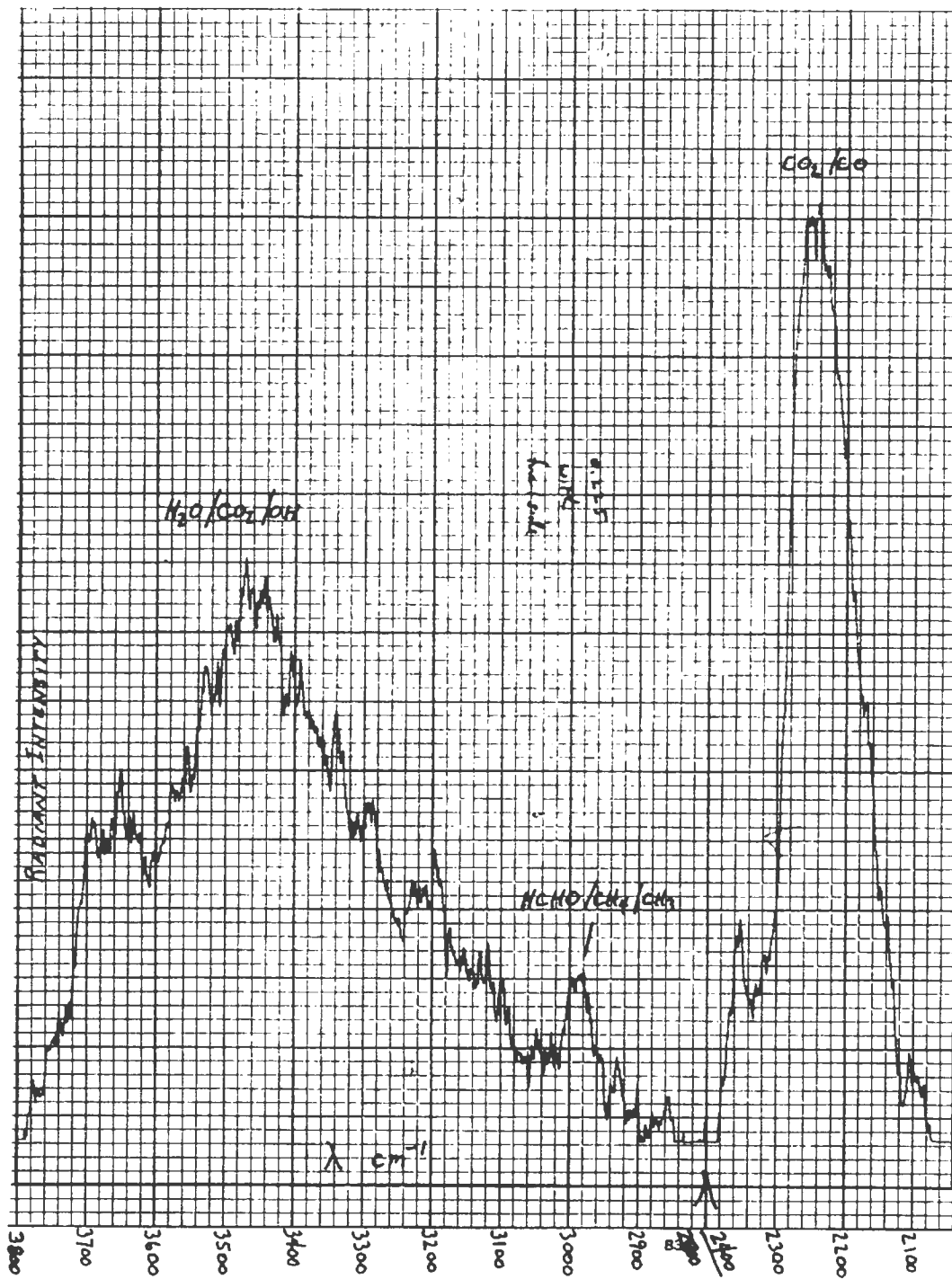


Figure 7b. Infrared Emission of Methane/Air Opposed-Jet Diffusion Flame - Flame Center

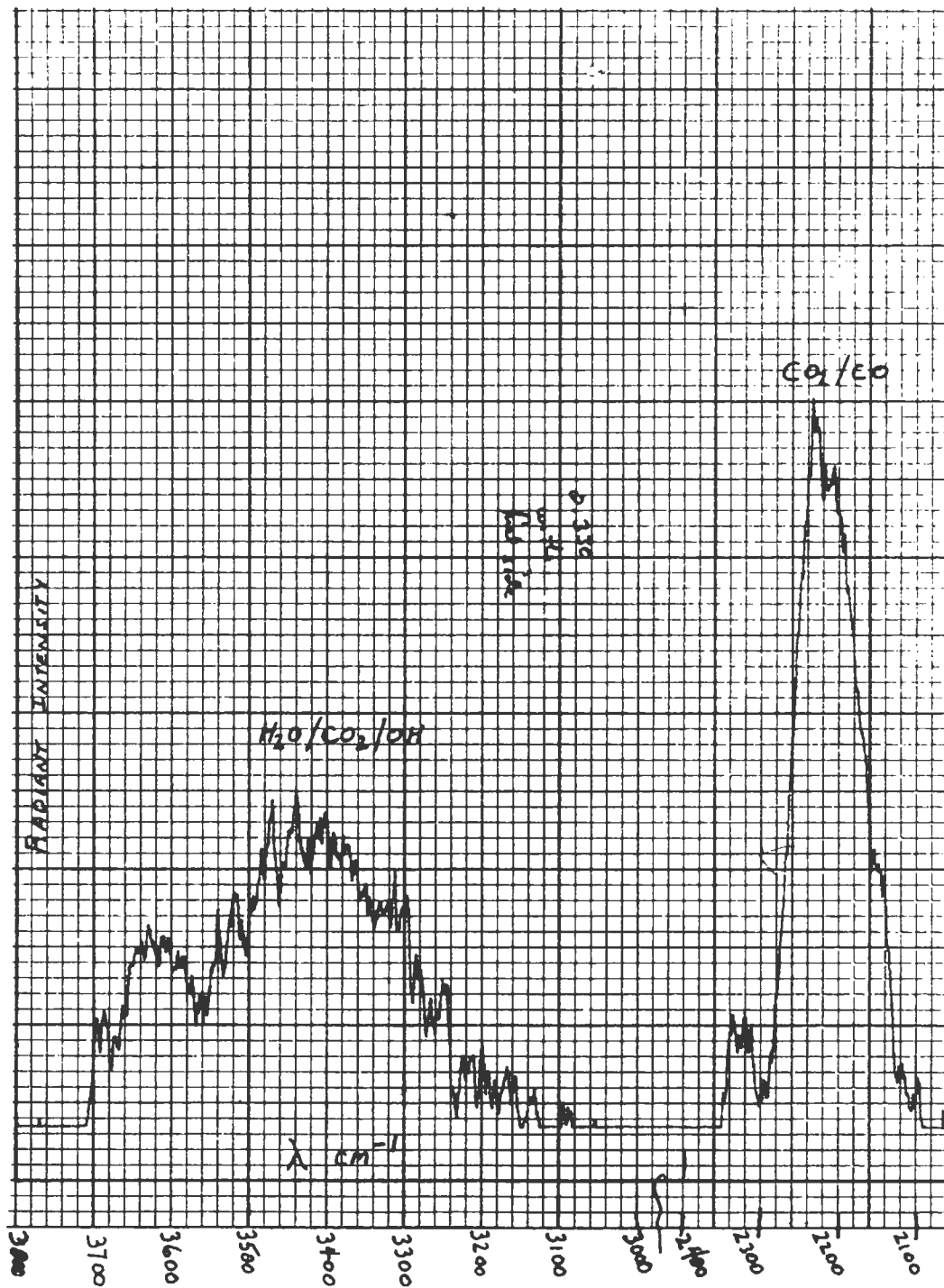
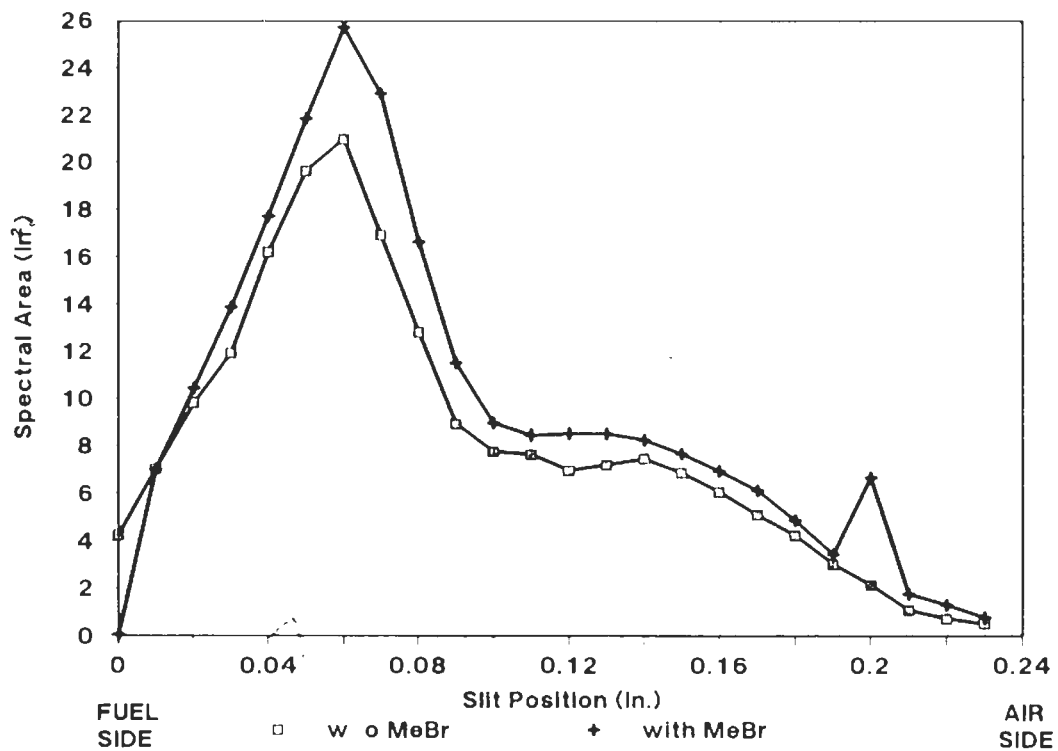


Figure 7c. Infrared Emission of Methane/Air Opposed-Jet Diffusion Flame - Air Side

# Figure 8

IR Spectral Emission of Methane Flame  
1.6% Methyl Bromide Added to Air Side  
3700 - 2700  $\text{cm}^{-1}$



# Figure 9

IR Spectral Emission of Methane Flame  
1.6% Methyl Bromide Added to Air Side  
2450 - 2000  $\text{cm}^{-1}$

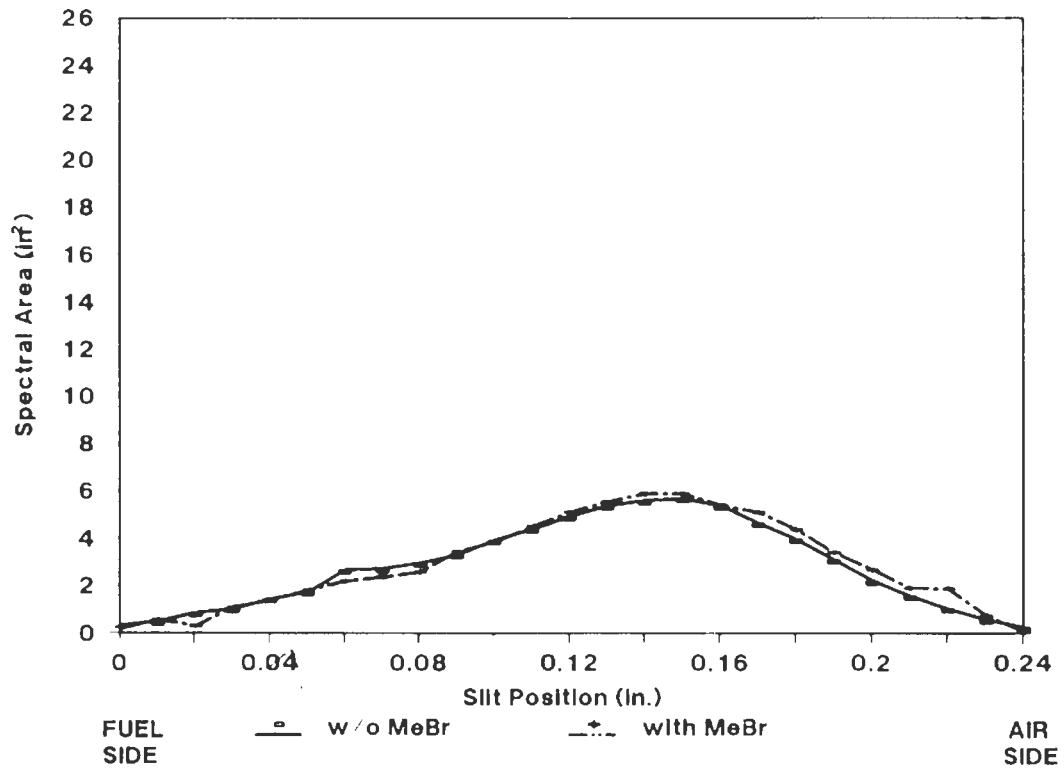


# Figure 10

IR Spectral Emission of Methane Flame  
1.6% Methyl Bromide Added to Air Side  
Peak at  $3470\text{ cm}^{-1}$

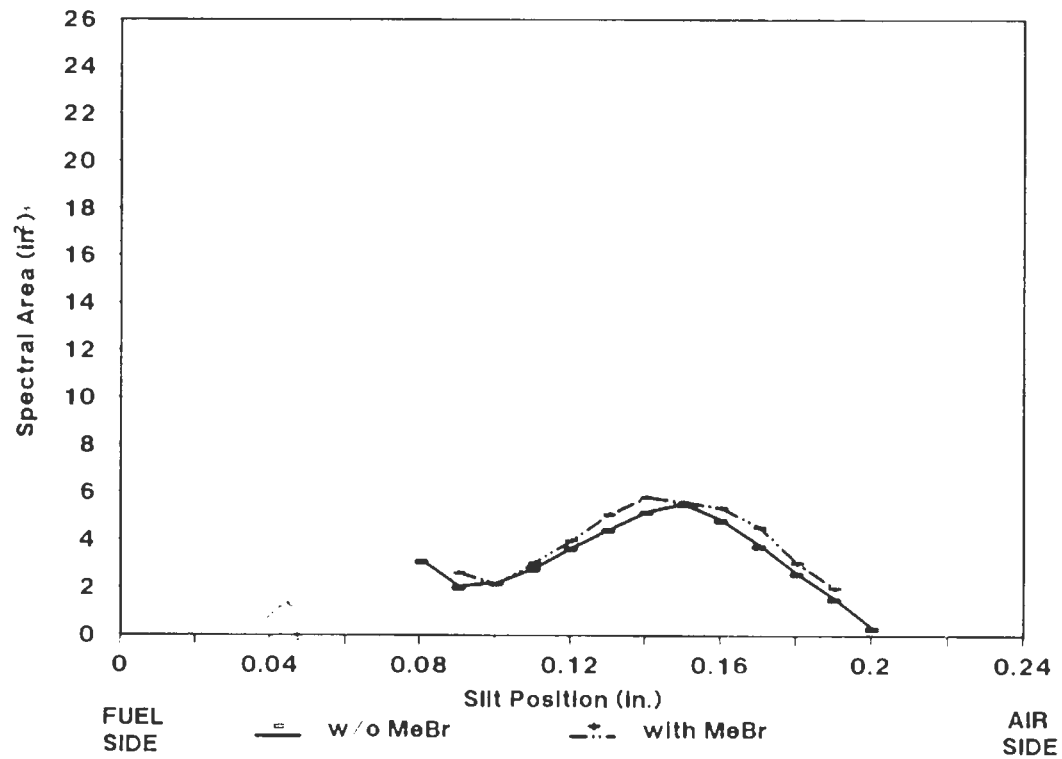


# Figure 11

IR Spectral Emission of Methane Flame  
1.6% Methyl Bromide Added to Air Side  
Peak at  $3000\text{ cm}^{-1}$

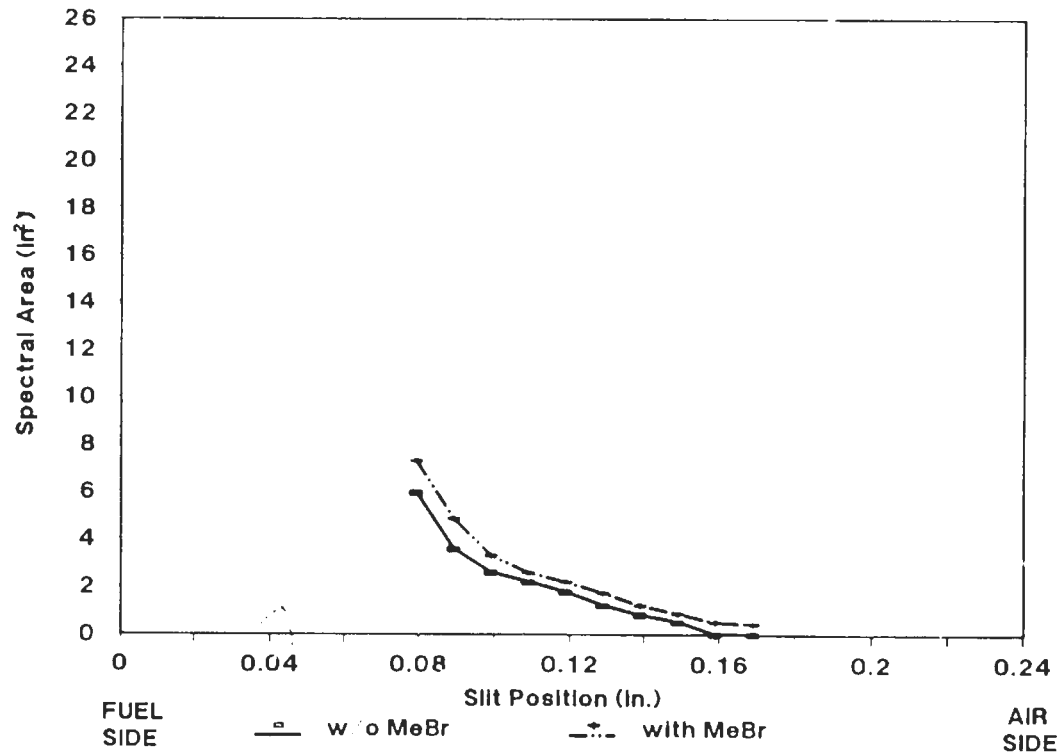


# Figure 12

IR Spectral Emission of Hydrogen/Carbon Monoxide Flame  
100 ppm Phosphorus Pentoxide  
3800 - 2700  $\text{cm}^{-1}$

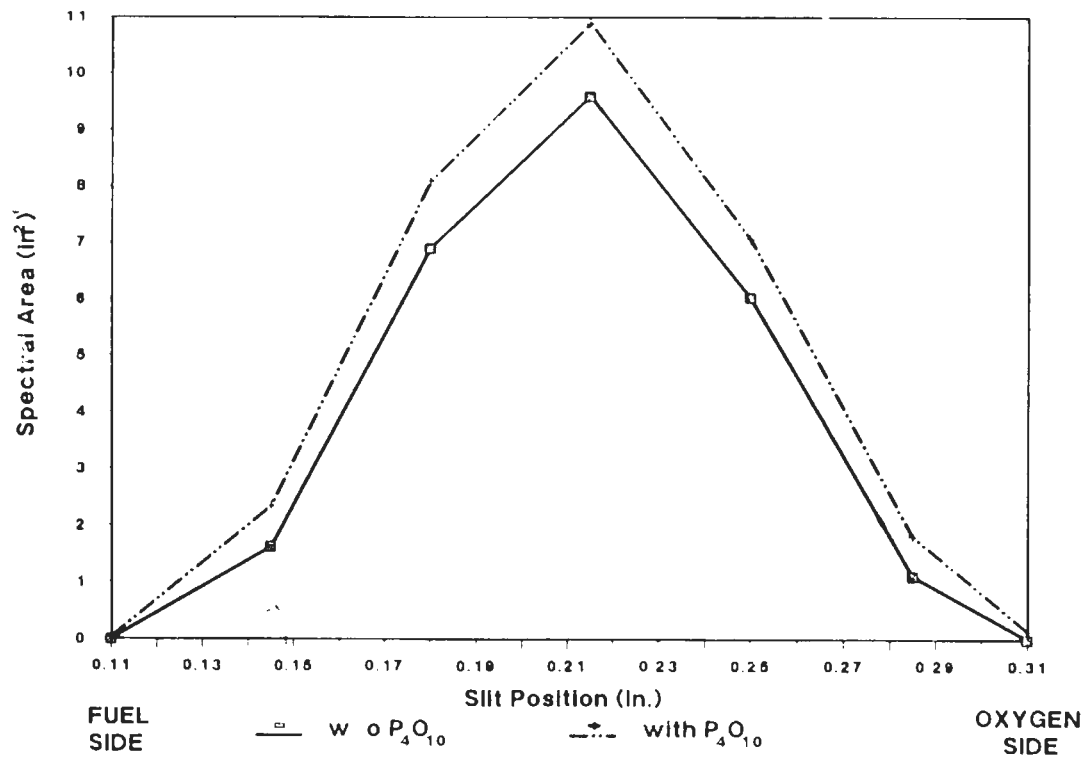


# Figure 13

IR Spectral Emission of Hydrogen/Carbon Monoxide Flame  
100 ppm Phosphorus Pentoxide  
2450 - 2000  $\text{cm}^{-1}$

